Republic of Iraq
Ministry of Higher Education and Scientific Research
University of Misan/College of Engineering
Department of Civil Engineering

Enhancement of Flexural Performance for RC Beams with Different Configuration of Steel Reinforcement

A THESIS

Submitted in Partial Fulfillment of the

Requirements for the Degree of

Master of Science/Master of Structural Engineering

(in Civil Engineering)

By

Fatima Aboud Kareem

B.Sc. civil engineering, 2020

Advisor Name: Prof. Dr. Sa'ad Fahad Resan

ذو الحجة 1446 June 2025

بسم الله الرحمن الرحيم

يَرْفَعِ اللَّهُ الَّذِينَ آمَنُوا مِنكُمْ وَالَّذِينَ أُوتُوا الْعِلْمَ دَرَجَاتٍ وَاللَّهُ بِمَا تَعْمَلُونَ خَبِيرٌ ۝

صدق الله العلي العظيم

من سورة المجادلة

Abstract

This thesis investigates the influence of steel reinforcement configurations on the mechanical properties and ultimate strength of reinforced concrete (RC) beams, with a particular focus on enhancing ductility and energy absorption capabilities. Given the inherent brittleness of concrete, this research aims to explore how various reinforcement geometries can significantly improve structural performance under load. A series of experimental tests were conducted involving fourteen simply supported RC beams subjected to two central point loads. The beams were designed with varying amounts and configurations of longitudinal reinforcement, including straight, curved, and triangular forms. The results demonstrated a significant range in ultimate load capacities, from 184 kN to 284.82 kN, with corresponding displacements between 20.48 mm and 34.88 mm. Particularly noteworthy was the introduction of curved steel reinforcement, which led to a marked enhancement in the ultimate load and ductility index. The beam with five curved rebars displayed a 32% increase in ultimate load capacity and a ductility index of 4.07, reflecting a 22.2% improvement over the control beam. The analysis further reveals that the configuration of reinforcement plays a pivotal role in the performance of RC beams. Curved reinforcement configurations were found to significantly improve both cracking and ultimate loads, suggesting that this geometry enhances the bond between concrete and steel, facilitating better load distribution and resistance to initial cracking. In contrast, triangular reinforcement configurations yielded lower overall performance metrics, although they still provided some benefits in terms of structural integrity. Energy absorption capacity, a crucial factor in assessing the resilience of structures, was also notably enhanced with the use of curved rebars. The maximum observed energy absorption reached 3492.63 kN.mm in the beam

reinforced with five curved rebars, indicating an increase of 84.6% over the control beam. This finding highlights the effectiveness of curved reinforcement in dissipating energy during loading. Additionally, the relationship between compressive strength and mechanical performance was explored. Higher compressive strength materials were shown to improve both cracking load and ultimate load capacity, emphasizing the importance of material strength in determining the overall effectiveness of reinforced concrete structures. The findings suggest a synergistic effect between the curvature of reinforcement and the compressive strength of concrete, collectively enhancing the structural integrity and load-carrying capacity of the beams.

SUPERVISOR CERTIFICATION

I certify that the preparation of this thesis entitled " **Enhancement of Flexural Performance for RC Beams with Different Configuration of Steel Reinforcement**" was presented by " Fatima Aboud Kareem ", and prepared under my supervision at the University of Misan, Department of Civil Engineering, College of Engineering, as a partial fulfillment of the requirements for the degree of Master of Science in Civil Engineering (Structural Engineering).

Signature:

Prof. Dr. Sa'ad Fahad Resan

Date:

In view of the available recommendations, I forward this thesis for discussion by the examining committee.

Signature:

Assist Prof. Dr. Murtadha Abbas Abd Ali

(Head of Civil Eng. Department)

Date:

EXAMINING COMMITTTEE'S REPORT

We certify that we, the examining committee, have read the thesis titled " **Enhancement of Flexural Performance for RC Beams with Different Configuration of Steel Reinforcement** " which is being submitted by (Fatima Aboud Kareem), and examined the student in its content and in what is concerned with it, and that in our opinion, it meets the standard of a thesis for the degree of Master of Science in Civil Engineering (Structures).

Signature:
Name: **Prof. Dr. Sa'ad Fahad Resan**
(Supervisor)
Date: / /2025

Signature:
Name:
(Co-supervisor)
Date: / /2025

Signature:
Name: Full name with scientific rank
(Chairman)
Date: / /2025

Signature:
Name: Full name with scientific rank
(Member)
Date: / /2025

Signature:
Name: Full name with scientific rank
(Member)
Date: / /2025

Approval of the College of Engineering:
Signature:
Name: Full name with scientific rank
Dean, College of Engineering
Date: / /2025

DEDICATION

- To the first teacher, Muhammad (may God's blessings be upon him and his family),
- To my beloved homeland,
- To those who raised me—my parents, my siblings, and my dear husband,
- To all those who supported and helped me, made the difficult easy, especially my supervisor

Prof. Dr. Sa'ad Fahad Resan ,

- To my colleagues and everyone who contributed to the completion of this research,

I dedicate the fruits of my hard work.

ACKNOWLEDGEMENTS

All praise and thanks are due to Allah alone, and peace be upon the one sent as a mercy to the worlds, Muhammad, the trustworthy Prophet, and upon his pure and righteous family.

As an expression of gratitude and appreciation, I extend my heartfelt thanks and deep respect to my esteemed professor and I sincerely thank my supervisor, **Prof. Dr. Sa'ad Fahad Resan** for his continuos guidance and support, whose invaluable guidance, knowledge, and insightful suggestions have greatly contributed to shaping this research with the necessary depth and academic rigor. May Allah reward him abundantly.

I also extend my sincere appreciation to **Prof. Dr. Abbas Oda Dawood** , Dean of the College of Engineering at the University of Misan, and **Assist. Prof. Dr. Murtada Abass Abd Ali**, Head of the Civil Engineering Department, for their continuous support and assistance.

TABLE OF CONTENTS

LIST OF TABLES

LIST OF FIGURES

LIST OF SYMBOLES

RC: Reinforced Concrete

F: Load (Force)

D: Ductility Index

E: Energy Absorption

Δu: Ultimate Deflection

Δy: Yield Deflection

Fcu: Compressive Strength for cubes

kN: Kilonewton

mm: Millimeter

MPa: Megapascal

l: Length

d: Depth of Beam

ρ: Reinforcement Ratio

σ: Stress

ε: Strain

μ: Poisson's Ratio

α: Coefficient of Thermal Expansion

V: Shear Force

LIST OF ABBREVIATIONS

ASCE : American Society of Civil Engineer

RC: Reinforced Concrete

ACI: American Concrete Institute

ASTM: American Society for Testing and Materials

MPa: Megapascal

kN: Kilonewton

kN.mm: Kilonewton millimeter

D: Ductility Index

DSB : Double – slotted Beam

Fcu: Compressive Strength

B: Beam

BCFS: Beam Control with Straight reinforcement

BCF: Beam with Curved reinforcement

BTF: Beam with Triangular reinforcement

E: Energy Absorption

L: Load

Δu: Ultimate Deflection

Δy: Yield Deflection

CHAPTER ONE: INTRODUCTION

1.1 General

In recent years, there have seen an increasing acknowledgement of the need for a logical and economical design methodology for statically indeterminate structures, including the inelastic deformation of structural materials. This deformation causes a redistribution of internal moments and forces inside the structure, resulting in a substantial enhancement of its strength beyond what would be attained by only considering elastic deformation. Nevertheless, reinforced concrete, being a brittle material, has limited inelastic deformation capacity. Thus, there may be instances when the deformation capacity at certain crucial portions is depleted prior to the complete redistribution of internal moments throughout the structure[1]. Consequently, it is essential to define recognised safe thresholds for deformation capacity. The integration of inelastic deformations into the design methodologies of concrete structures has been the subject of comprehensive experimental and analytical investigations. Researchers have invested considerable effort in comprehending and characterizing the behaviour of concrete structures subjected to inelastic deformation. Theis study seek to provide design methodologies that guarantee sufficient strength and performance while accounting for the constraints of concrete's inelastic deformation capability. Incorporating inelastic deformations into the design process enables engineers to create more efficient and cost-effective designs for statically indeterminate structures. This method optimizes the structural material's strength and offers a more precise depiction of the structure's performance under diverse loading circumstances [2]. Experimental and analytical study findings are essential for enhancing design methodologies and recommendations for concrete buildings, therefore assuring their safety, durability, and overall performance. Numerous analytical design methodologies, known as limit design theories, have

been suggested. The theories primarily seek to provide a solution by fulfilling the equilibrium and deformation compatibility conditions of the structure at ultimate, based on an understanding of the load deformation characteristics of its elements. Either the moment-curvature link, which has been provided by Guyon [3], Macchi [4], Sawyer [5], and Lee [6], or the moment-rotation relationship, which has been defined by A.L.L. Baker [7] and Gartner [8], are the foundations upon which theories are built. The data that was obtained from the tests that were carried out indisputably reveals that the moment-curvature relationship, which was calculated at the essential part, is not sufficient to be used as a representation of the member's overall behaviour. Because of this shortcoming, it became clear that the problem needed to be addressed by gaining a knowledge of the link between moment and rotation. The ultimate load theory of design, initially articulated by Baker and further endorsed by the Institution of Civil Engineers Research Committee and the European Concrete Committee, represents one of the most comprehensive approaches in structural engineering. This methodology is grounded in the principle of moment rotation, which effectively captures the behaviour of structural elements under varying load conditions. Over the years, the theory has undergone significant refinement and development, enhancing its applicability to real-world scenarios. As a result, it provides engineers with a robust framework for predicting the performance of structures, allowing for more informed design decisions that prioritise safety and efficiency. Its evolution reflects a growing understanding of complex interactions within materials and load-bearing systems, making it an essential tool in modern structural design practice. This advancement contributes to improved structural integrity and supports the sustainable development of engineering solutions tailored to contemporary challenges. The study demonstrated that varying steel reinforcement configurations significantly affects the ultimate strength and mechanical properties of reinforced concrete (RC) beams. Specifically, the introduction of curved and

triangular reinforcement resulted in notable differences in cracking load, ultimate load, and overall structural behaviour. These variations indicate that reinforcement design plays a crucial role in enhancing the performance of RC beams. The utilization of curved reinforcement led to substantial improvements in cracking and ultimate loads. For instance, the transition from straight to curved rebar resulted in increased loads and deflections, demonstrating that curved configurations enhance load distribution and bond strength between steel and concrete. This enhancement indicates that curving the rebar can effectively improve the structural integrity of beams, making them more resilient under applied loads.

1.2 Rotation Capacity

The rotation capacity (θ_p) is the maximum angle that the beam can rotate at the plastic hinge before failure. θ_p depends on the ductility and confinement of the beam, as well as the strain hardening and buckling of the steel. There are different methods to calculate θ_p, such as the ones proposed by Bracci et al. (1997) [9] and Priestley et al. (2007) [10]. For example, the method by Bracci et al. is:

$$\theta p = \theta y + 0.08(\mu - 1) \quad \text{.....(1)}$$

In this context, θy represents the rotation at yield, while μ denotes the ductility factor, defined as the ratio of the ultimate displacement to the yield displacement of the beam. The plastic hinge length Lp is the distance measured from the face of the support or the zero moment point to the location where the curvature of the beam equals its yield curvature. This length is influenced by various factors, including the geometry of the beam, its material properties, and the reinforcement ratio. To estimate Lp, several empirical formulas have

been developed, notably those introduced by Paulay and Priestley in 1992 [11], as well as Park and Paulay in 1975 [12]. For instance, the formula proposed by Paulay and Priestley provides a means to calculate Lp based on specific design parameters, helping engineers predict behaviour under loading conditions and ensuring structural safety. Understanding these relationships is crucial for effective design, as it enables engineers to optimise beam performance and enhance overall structural resilience.

$$L_p = 0.08Z + 0.022 f_y\, dp \geq 0.044 f_y\, dp \quad \ldots\ldots\ldots\ldots\ldots\ldots\ldots\ldots\ldots\ldots (2)$$

where Z is critical distance from the critical section to the point of contraflexure, f_y is the yield strength of steel, and dp is the bar diameter .

There are a variety of factors that can affect the plastic hinge length and rotation capacity of reinforced concrete beams. For example, the concrete strength and quality can influence cracking and crushing behaviour, while the steel reinforcement ratio, layout, and detailing can affect yield moment, strain hardening, and buckling. Additionally, the shear span ratio (the distance from the support to the point of maximum moment divided by the effective depth of the beam) can reduce Lp and θp with a lower ratio. Lastly, loading history and pattern also play a role in determining the amount and direction of cyclic loading and displacement that the beam experiences. The plastic hinge length and rotation capacity of reinforced concrete beams can be measured experimentally or numerically.

approaches that align with the principle that the rotation at the plastic hinge must exceed the rotation required for structural performance. The rotation of the plastic hinge, denoted as θp, in reinforced concrete beams is influenced by a

multitude of factors. These include the definitions of yielding and ultimate curvatures, the geometry of the section, material properties, and the ratios of both compression and tension reinforcement . Additionally, the effects of transverse reinforcement, cracking behaviour, and tension stiffening play critical roles in determining θp. Other significant considerations encompass the stress-strain relationships for both concrete and reinforcing steel, as well as the bond-slip characteristics that arise at the interface between these two materials. Support conditions, the magnitude and type of loading, axial force, loading plate width, shear effects, and the presence of columns are also essential elements that contribute to the overall behaviour of the plastic hinge . Understanding these factors is vital for accurately predicting the rotational capacity of reinforced concrete beams, ensuring that they can withstand the demands of various loading scenarios while maintaining structural integrity. This holistic approach to design and analysis ultimately enhances the safety and performance of concrete structures in engineering applications. Despite the fact that this issue has been studied by several experts, there is still no universally accepted description of the plastic rotation capacity. Researchers' divergent views on what constitutes an ultimate limit state, as well as variations in test parameters like specimen size, loading plate shape, application technique, and load types, contribute to these apparent inconsistencies. The plastic hinge length and inelastic rotation capacity can be calculated using certain formulae; however, there is still no consensus on how to assess the inelastic behavioural properties of undetermined concrete constructions. In Fig. 1.1, we can see the circumstances at the ultimate load stage of a standard cantilever beam that is loaded uniformly. The cantilever's curvature grows progressively from point A, the free end, to point B, the column face, for values of weights less than the yielding moment. At first yield, the curvature of tension steel increases significantly. Large inelastic deformations are caused by a rapid rise in the value of the support's curvature at the

ultimate load stage. Along the length of the beam, the curvature varies because tension-stiffening is possible in the concrete between the fractures. The spots where cracks appear are shown by the peaks of curvature. Total rotation, θ t, along the length of the beam may be separated into elastic, θe, and plastic, θp, rotations, based on the idealisation of the distribution of curvature at the ultimate load stage, which can be seen in Figure 1.1 (c) as elastic and inelastic (plastic) areas, respectively. The curvature at yielding may be used to determine the elastic rotation, θe, which is the time it takes for the steel to yield.

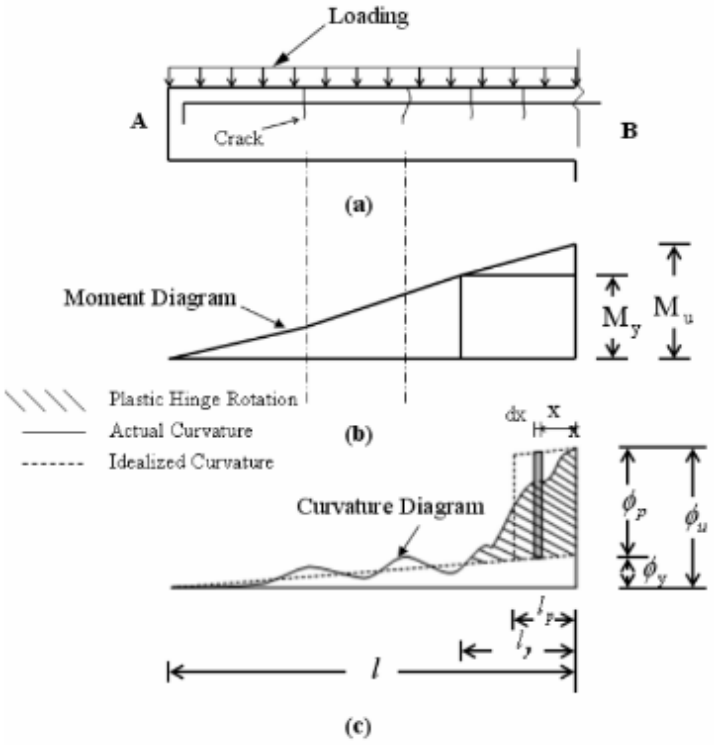

Fig.1.1 Curvature Distribution along the Beam according to the Schematic at the Final Stage: Beam, Bending Moment Diagram, and Curvature Diagram are the three types of diagrams [15].

1.3 Plastic Hinge Analysis

The crack curvature can be effectively produced by following the guidelines of the CEB-FIP Code [13], along with considerations for rebar distribution and the relationship between tensile force and curvature, as illustrated in Figure 1.2. To calculate the crack distance, a specific formula can be employed. The contribution of concrete in the segments between cracks is assessed for each beam section by repeatedly solving the differential equation governing the bond behaviour, utilising a modified approach based on the methods described in the preceding section [14]. To estimate the curvature distribution between cracks, the distance from the tensile reinforcement to the neutral axis is determined, relying on the anticipated distribution of steel strain, as depicted in Figure 1.1. This measurement is critical for accurately assessing the curvature distribution across the beam, providing vital insights into how the structural elements behave under load. By integrating these calculations, engineers can gain a clearer understanding of the performance characteristics of reinforced concrete beams, ultimately leading to more informed design decisions that enhance structural integrity and durability.

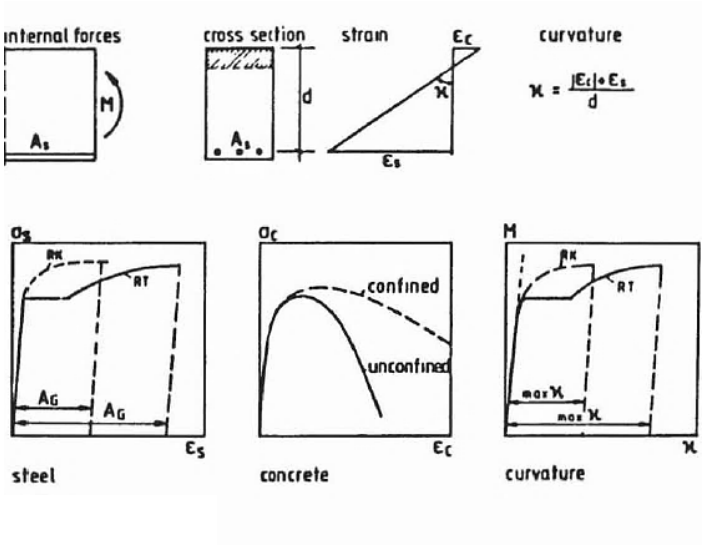

Fig. 1.2 Stress and Curvature Analysis in Reinforced Concrete Sections [14].

The rotation capacity of the beam may be determined by integrating these curvatures over the length of the beam. This technique is known as "integration".The plastic rotation may be defined as the difference between the rotation at the ultimate load and the rotation at a load that causes the reinforcement to yield at the place of maximum moment (for a further explanation, refer to Figure 1.3). This is a simple definition that can be used to describe the plastic rotation. In order for the mathematical model to be able to produce findings that can be relied upon, it is necessary that the behaviour of the material be characterised with a high degree of accuracy. Because of this, the stress-strain connection of the reinforcing steel is represented by a polygon with multiple segments, which makes it possible to depict the material's behaviour in a manner that is very accurate [14].

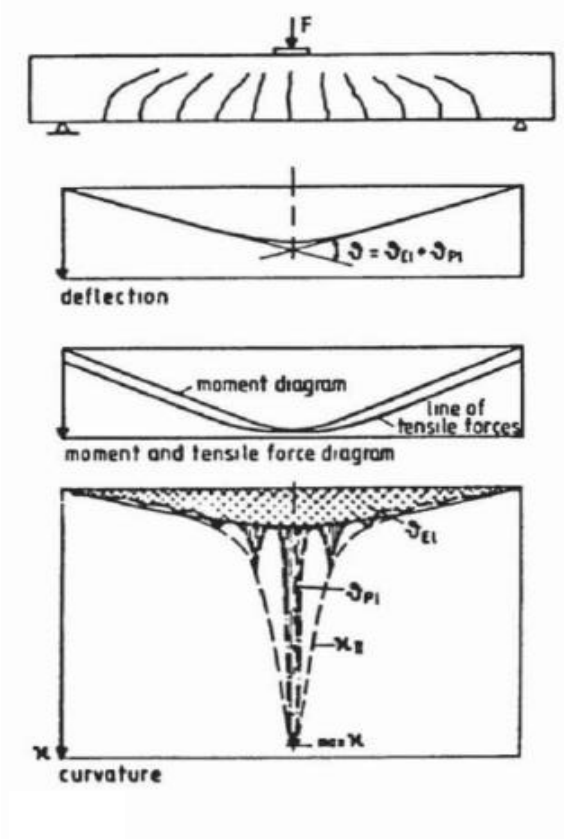

Fig. 1.3 Plastic Hinge Mathematical Model [14].

1.4 Objectives

This experimental investigation aimed to contribute more information about evaluating the plastic rotation capacity and ultimate strength of reinforced concrete beams. It is well acknowledged that the brittleness of the concrete significantly restricts the plastic rotation capability of these parts. Nevertheless, it is clear that this capability may be significantly enhanced with sufficient reinforcement in a multi-configurational setup. A substantial experimental study was conducted to investigate the impact of primary reinforcement on the plastic behaviour and deformation capacity of concrete since there has been little research on this parameter's evaluation. Two additional critical parameters, the influence of compressive strength steel configuration, are also examined in the experimental study. In order to study the impact of primary reinforcement, three sets of fourteen beams with varied longitudinal reinforcement quantities and multi-configurations were tested under a central point load.

1.5 Thesis Layout

This thesis has five chapters, summarized as follows:

1) Chapter one presents an overview of the topic.
2) Chapter two presents a comprehensive overview of prior research conducted on reinforced concrete beams examining their plastic rotation capability.
3) Chapter three, provides the experimental and analytical components of the thesis, including laboratory work and resolution of theoretical concepts.
4) Chapter four Focuses on analyzing the data, study findings, and discussion
5) Chapter five offerings the conclusions and recommendations for future work.

CHAPTER TWO: LITERATURE REVIEW

2.1 Introduction

In recent years, there has been an increasing recognition of the requirement for a rational and cost-effective design approach for statically indeterminate structures. This approach acknowledges the inelastic deformation of structural materials, which leads to a redistribution of internal moments and forces within the structure. As a result, the structure's strength significantly increases beyond what would be achieved by considering only elastic deformation. However, it is important to note that reinforced concrete, being a brittle material, has a limited capacity for inelastic deformation. Consequently, there may be situations where the deformation capacity at specific critical sections is exhausted before achieving a full redistribution of internal moments throughout the structure.

2.2 Rotation capacity and plastic hinge

Mendis [15] conducted research in the year 2001 to determine the plastic hinge lengths of standard and high-strength concrete while it was under flexure. The study was based on examining concrete samples as shown in fig (2.1) . This article presents a reexamination of previously established formulae, as well as a discussion of the influence of various factors on hinge length. A comparison was made between the values that were measured experimentally and the values that were anticipated by utilising these formulas. The upper and lower limits that were proposed by the ACI committee 428 [16] were found to produce valid estimations of hinge lengths for both standard and high-strength concrete flexural hinges up to 80 MPa. This was shown by the studies that were conducted. When it came to determining the length of the hinge, the results showed that equations that were derived from experimental findings were more dependable. The hinge lengths that were anticipated by the

majority of the equations were found to be within the limitations that were established by the ACI Committee 428 [17]. This was evident from both the results of the human studies and the computer experiments. In addition, a single phrase is not as appropriate for hinge length considerations as a stated range. In light of the findings of this research, it was advised that the hinge length determined by the envelope that was specified by the ACI limitations. When it comes to a softening structure, the hinge length ratio, which is represented by the letter m, is inversely related to the extremely important softening slope. According to the definition, the hinge length ratio is the ratio that is calculated by dividing the total length of a member by the hinge length. In 1986, Mendis [17] demonstrated that this link does in fact exist. Because of this, the effects of softening are significantly more noticeable for hinge lengths that are shorter. As a result of the fact that it is a particular quantity, the ACI limit below for hinge length is the kind of input value that is helpful for softening analysis. It is possible to locate additional information regarding the softening study of standard strength and high strength concrete buildings in other sources (Mendis, 2000) [18]. There is a high degree of accuracy that may be achieved when estimating hinge lengths for high-strength concrete beams (up to 80 MPa) and columns with low axial loads, as stated by the American Concrete Institute (ACI) [16]. In order to verify this discovery for columns that are subjected to large axial loads and for concretes that have a very high strength, more investigation is necessary.

An investigation on the flexural, axial load, and elongation response of plastic hinges as they were used in reinforced concrete members was given by Rajesh and colleagues [19] in the year 2007.

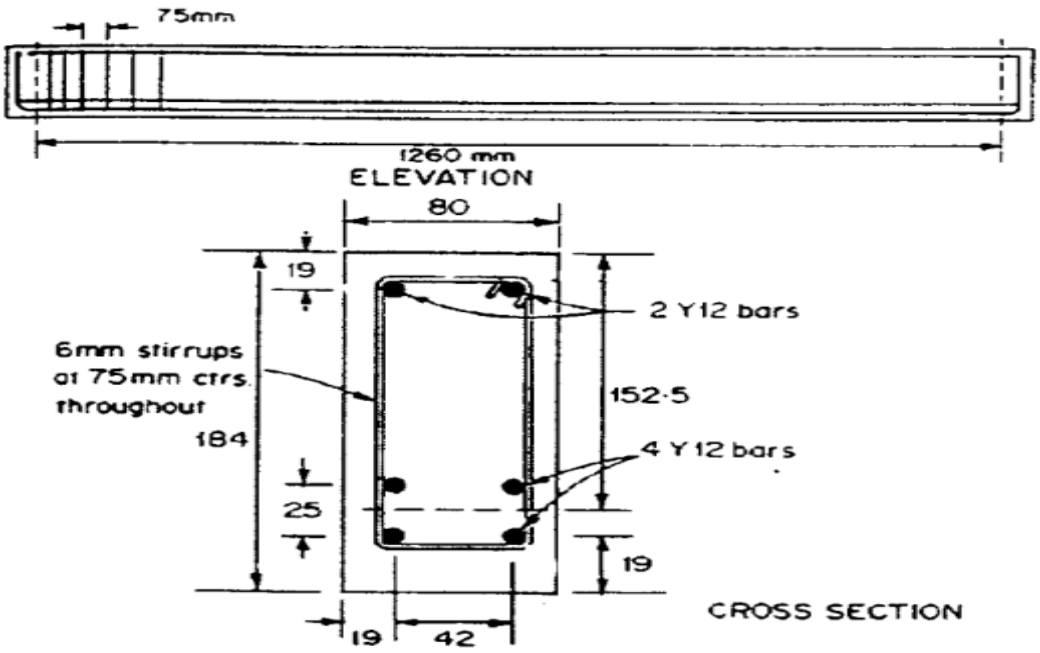

Figure 2.1: Specimens tested by Mendis [15]

In order to make predictions about elongation, a variety of empirical formulae have been discussed. On the other hand, there are presently no analytical models that are available that are sufficient and can be utilised to attempt to forecast the impact that elongation has on the seismic performance. The primary objective of this article was to present a comprehensive overview of a plastic hinge model specifically created to forecast the complex interactions of flexural, axial loads, and elongation behavior in plastic hinges within the context of reinforced concrete (RC) beams. This model was designed to effectively represent the flexural, shear, and elongation responses of a plastic hinge. It employed a filament-type element structure, which consisted of multiple layers of axial springs strategically arranged both diagonally and longitudinally. This innovative configuration allowed for a more accurate simulation of the physical behavior of plastic hinges under varying loading conditions. This layout allows the model to accurately depict the aforementioned responses. When comparing the data gained through experimentation with the analytical predictions

that were generated for beams with varied degrees of axial load, a comparison is done between the two sets of findings. Following an in-depth investigation, it has been demonstrated that the plastic hinge model provides an appropriate prediction of the reaction. The recently manufactured component makes it possible to conduct seismic evaluations, which can be utilized to ascertain the influence that beam elongation has on the seismic performance of reinforced concrete buildings. In a later stage, the model is going to be developed such that it can handle shear deformation that is associated with the expansion of shear reinforcement as well as the influence of axial force on the length of the plastic hinge. Both of these aspects was able to be accounted for by the model, as indicated by this circumstance. One of the potential used of this model was the study of the influence that elongation had on the seismic performance of reinforced concrete structures. This is one of the prospective applications.

In 2011, Zhao et al. [20] carried out research focused on the length of the plastic hinge in reinforced concrete flexural members. They developed and validated a computational model utilizing experimental data, which incorporated key aspects such as load-deflection responses, rotational capacities, and strain and stress distributions of the reinforcement. This model was constructed based on the insights gained from the experimental data. Using a numerically calibrated FE model, the researchers investigated various factors, including the actual length of the plastic hinge, the extent of the rebar yielding zone, the concrete crush zone, and the curvature localization zone. Parametric analyses were also conducted to explore the relationship between plastic hinge length and factors such as member dimensions, reinforcement ratios, and the material properties of both concrete and rebar. The findings demonstrated that a sophisticated FE model can effectively simulate the

complex behaviour exhibited by RC beams in the plastic hinge region. Due to the extensive parametric research conducted on the plastic hinge zone in RC members, this model can facilitate the derivation of formulas for calculating the plastic hinge lengths, denoted as Lpc and Lp.

In 2013, Palanivel and Sekar [22] conducted a detailed study on the flexural and plastic hinge behaviour of GFRP confined composite beams as shown in Fig (2.2). This research aimed to explore the interplay between flexural performance and plastic hinge behaviour in reinforced concrete beams that were enhanced with GFRP wraps and polyolefin fibres, particularly in critical sections known as the porous hinge zone. By incorporating stirrup confinement alongside these materials, the study sought to provide a comprehensive understanding of how these enhancements affect the structural integrity and performance of the beams under various loading conditions. The behaviour of the GFRP is affected by a variety of elements, including the proportion of polyolefin that is added, the number of layers that are used, and the way of wrapping (chopped or woven). This was done after the beams had been allowed to dry. When compared to confinement using lateral ties and FRP wraps, the incorporation of polyolefin fibres into GFRP-confined beams and lateral ties results in an improvement in performance under substantial deformations. The flexural performance of reinforced concrete beams was brought to a higher level by the utilization of fibres and the insertion of GFRP wraps. When compared to confinement obtained only through the use of lateral ties and FRP wrapping, the incorporation of polyolefin fibres into GFRP-confined beams and through the use of lateral ties results in an improvement in performance under considerable modifications. The results of the study showed that the post-peak behaviour of the FRPCFRC beams is improved in comparison to the nonfibrous FRP beams. This was found to be the case in terms of ductility. By incorporating fibres into the beams,

the augmentation of confinement was able to reduce the deterioration of strength and stiffness in the beams. This indicates that the material was able to keep its strength and stiffness despite enduring large deformations. The beam confinement process results in a significant improvement in both the strength and the ultimate strain of the material. The degree of confinement determines the extent to which the strength is increased by a factor ranging from 1.2 to 1.6 in comparison to the strength observed in the unconfined state. When compared to the unconfined strain, the failure strain is increased by a factor of ten to twenty. During both the pre-peak and post-peak stages of the load-deflection curves, the fibres led to an improvement in the cracking performance of the concrete. Both the numerical calculations and the experimental data were found to be in strong agreement with one another.

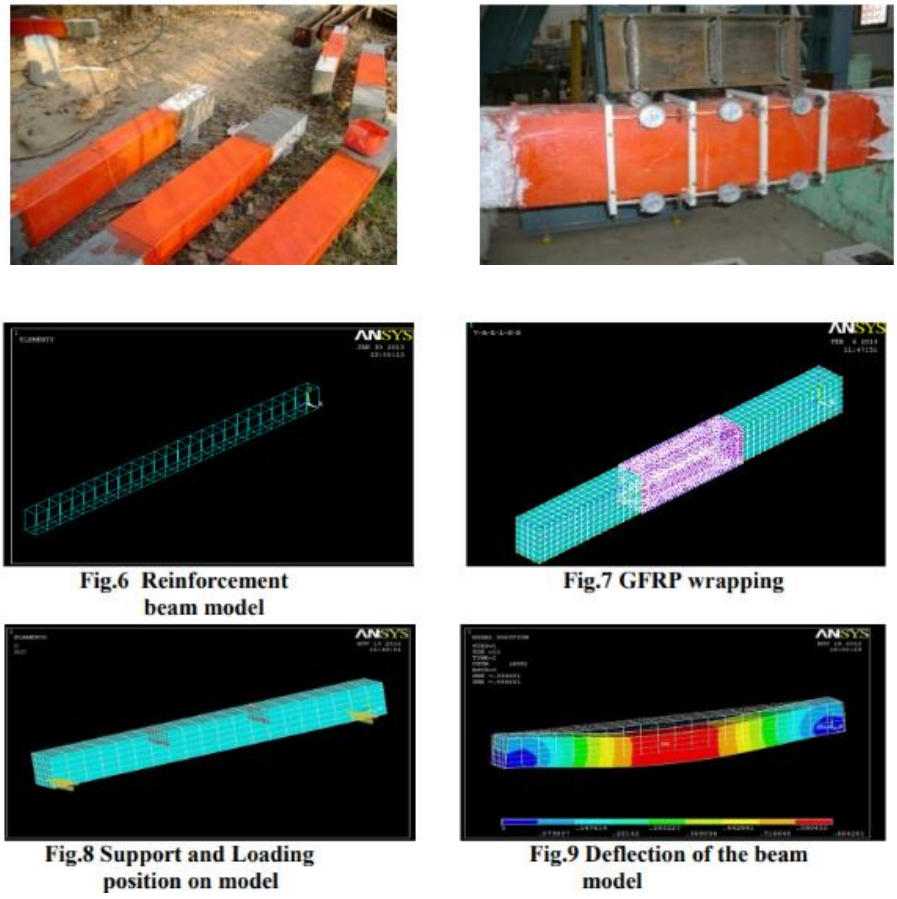

Figure 2.2: Specimens tested by Palanivel and Sekar [22]

In 2014, Oudah and El-Hacha [23] conducted an analysis of slotted-beam specifications to effectively reposition the centre of rotation at beam-column joints distally from the column face as in Fig 2.3. Their innovative connecting system featured a single vertical slit integrated into the underside of the beam. This study aimed to explore the implications of adjusting the vertical slot along the beam's length, thereby repositioning the plastic hinge within the reinforced concrete slotted-beam column connection. The evaluation was carried out on two distinct specimens. One specimen had a vertical slot situated directly at the column face, while the other featured a vertical slot placed away from the column face, specifically at a distance equivalent to the spacing between the top and bottom reinforcements. The test results revealed that the seismic shear demand in the specimen with the repositioned slot was greater than that of the specimen with the slot aligned at the column face. Furthermore, the curvature distribution analysis of the specimen with the relocated slot indicated that curvature peaks occurred near the site of the slot. This finding highlighted the effects of slot positioning on the structural performance of the connection, providing valuable insights into the behaviour of slotted-beam column connections under seismic loading conditions. The study underscored the significance of design modifications for enhancing the resilience of reinforced concrete structures.The findings demonstrate that repositioning the slot away from the column's face effectively relocated the plastic hinge. The augmentation of the ultimate load and the repositioning of the maximum curvature under both positive and negative bending demonstrated the efficacy of moving the plastic hinge. Observations of the fracture pattern during failure revealed that repositioning the plastic hinge further from the column face distributes plasticity across a greater distance.

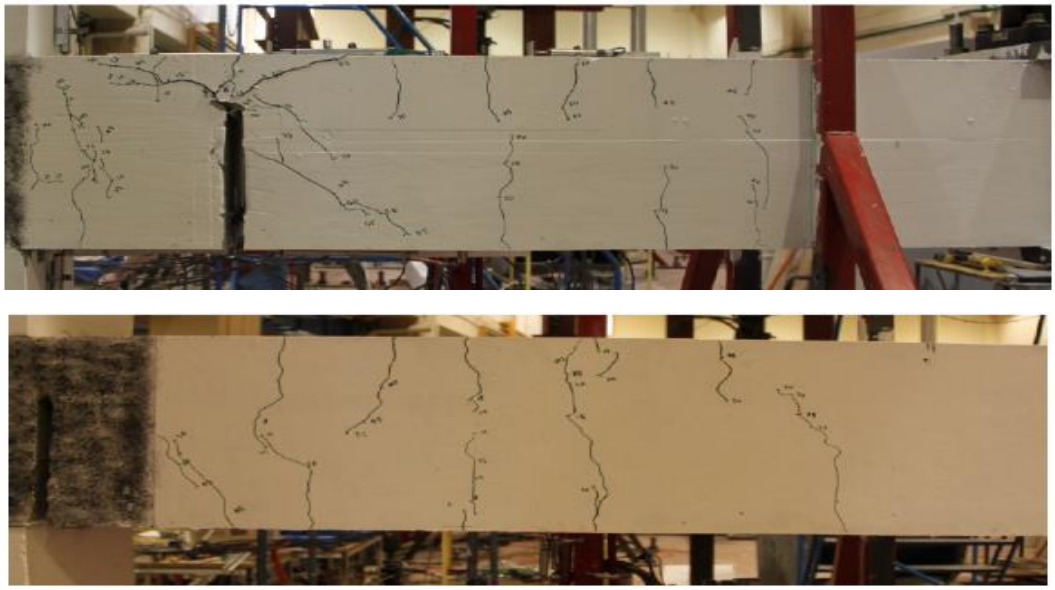

Figure 2.3: Specimens tested by Oudah and El-Hacha [23]

Ou and Nguyen [24] conducted an investigation of the length of the plastic hinges of reinforced concrete beams that had deteriorated in 2014. Through this study, the researchers investigated how the load-bearing capacity of reinforced concrete beams is affected by the corrosion of reinforcement. The experimental findings of corroded reinforced concrete beams were used to validate a non-linear finite element analysis approach that was developed. The Lp of reinforced concrete beams was investigated using a parametric research approach in order to determine the impacts of f'c, longitudinal tension, a/d, in addition to corrosion level. As a result of the findings of the investigation, it was discovered that the Lp had a modest correlation with the compressive strength of concrete and the longitudinal tension reinforcement ratio. On the other hand, it had a strong correlation with shear span for both uncorroded and corroded beams. In addition, the Lp reduced as the corrosion became more severe, indicating a substantial connection with the decrease in the flexural-strength hardening ratio that can be attributed to corrosion. Pitting corrosion led to several detrimental effects on structural materials, particularly in reinforced

concrete. One significant consequence was the reduction in the yield and ultimate strengths of steel, which compromised the material's ability to bear loads effectively. Additionally, pitting corrosion resulted in a decrease in ultimate strain, further diminishing the structural integrity and ductility of the steel components. Moreover, pitting corrosion modified the bond constitutive law between corroded steel bars and concrete in Fig 2.4. This alteration weakened the bond strength, affecting the overall performance of the reinforced concrete structure. As corrosion progressed, the interaction between the steel reinforcement and the surrounding concrete deteriorated, potentially leading to premature failure under load. Generally speaking, the amount of Lp decreases as the degree of corrosion increases. The decline occurs at a faster rate at higher corrosion levels (between 15 and 25 percent) in comparison to lower corrosion levels (between 0 and 15 percent).

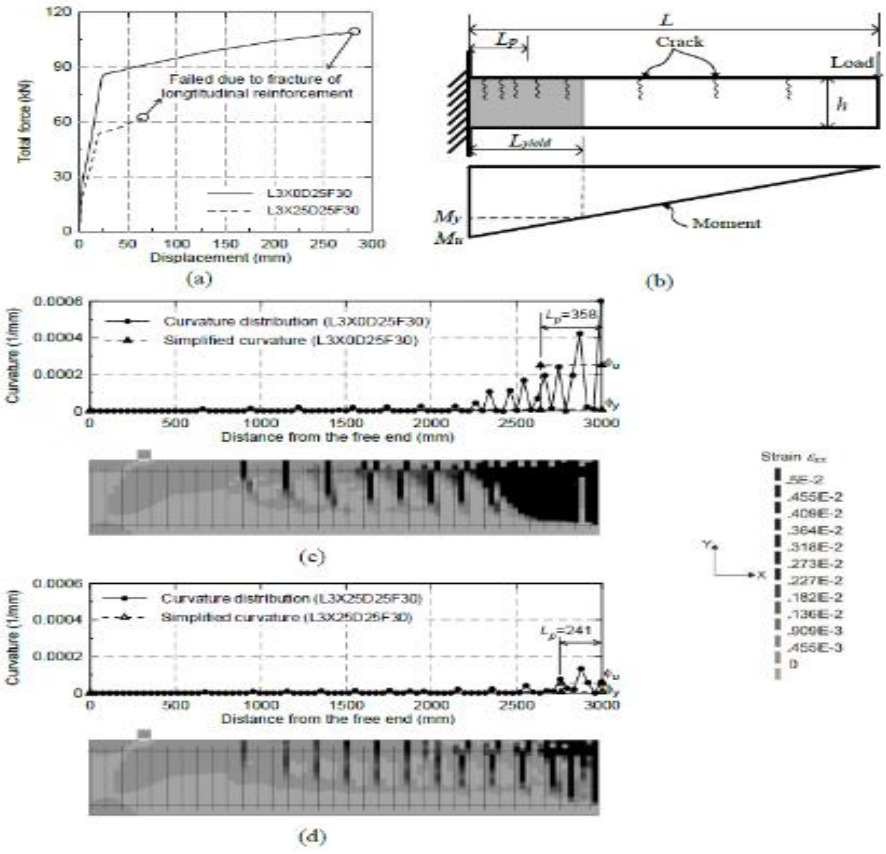

Figure 2.4: Specimens tested by Ou and Nguyen [24]

An examination of the impact behaviour of reinforced concrete beams was presented by Pham and Hao [25] in 2017. The investigation focused on the effect of the plastic hinge and boundary conditions on the beams. In this study, a quantitative investigation was conducted to investigate the impact that plastic hinges and boundary conditions have on the performance of reinforced concrete beams when they are subjected to scenarios with slow impact velocity. The displacement and damage of relatively long beams were significantly influenced by boundary conditions. When assessing the structural stiffness of a beam using a single degree of freedom model to predict impact loads, it was crucial to consider both the growth of the plastic hinge and its stationary position. This consideration was particularly important because, at high impact velocities, the model's effectiveness in calculating peak beam response became questionable, as it was not inherently dependent on the boundary conditions. The findings indicated that while the impact force remained largely unaffected by the presence of a plastic hinge or the specific boundary conditions, the displacement of relatively long beams was strongly impacted by these factors. This result was consistent with the impact velocities evaluated in this study, which ranged from one to twelve meters per second. Notably, there was no observable correlation between the boundary conditions of moderately long beams and the maximum impact force or its duration. The beam that was merely supported encounters a significant negative bending moment, which is something that needs to be taken into consideration. When compared to the peak displacement, the extent to which the boundary conditions influenced the residual displacement was significantly greater. After being subjected to an impact velocity of 12.89 meters per second, reinforced concrete beams exhibited indications of concrete scabbing. The manner in which the beams collapse is significantly impacted by concrete strengths ranging from 20 to 100 MPa; nevertheless, there is no discernable impact force or displacement that is influenced by these strengths as shown in Fig 2.5.

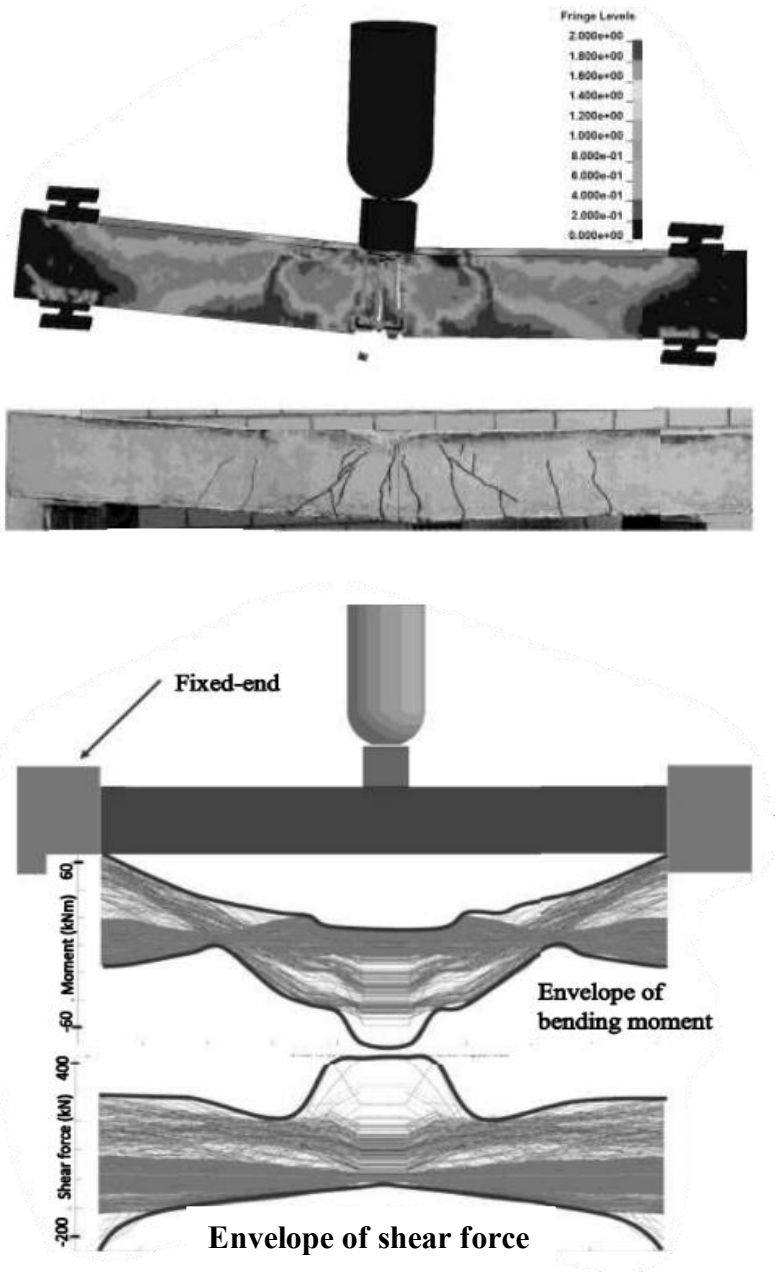

Figure 2.5: Specimens tested by Pham and Hao [25]

Oudah and El-Hacha [26] presented their findings from a research that was conducted in 2017 addressing the relocation of plastic hinges in concrete structures by utilizing the double-slotted-beam method. A novel concrete beam-column connection, termed the double slotted beam (DSB), was developed for this research to effectively relocate the plastic hinges installed in concrete frames. The design

allowed for high precision in positioning the centre of rotation. To manage this positioning, the DSB system incorporated two vertical holes cut into the top and bottom fibres of the beam member as in Fig 2.6. By repositioning the vertical slots away from the face of the column, the team aimed to enhance the adjustment of the plastic hinge. The experimental evaluation of large-scale DSB connections, both with and without the relocated vertical slots, revealed several important characteristics. These included impressive drift capabilities, non-tearing action, minimal concrete damage, and reduced bond deterioration at the joint.

The results highlighted that the DSB connections performed remarkably well under various loading conditions, showcasing their potential for improving the resilience of concrete structures. The innovative design not only contributed to maintaining structural integrity during seismic events but also indicated a significant reduction in maintenance needs over time. This research provided valuable insights into the effectiveness of the DSB system, paving the way for future applications in modern civil engineering practices.

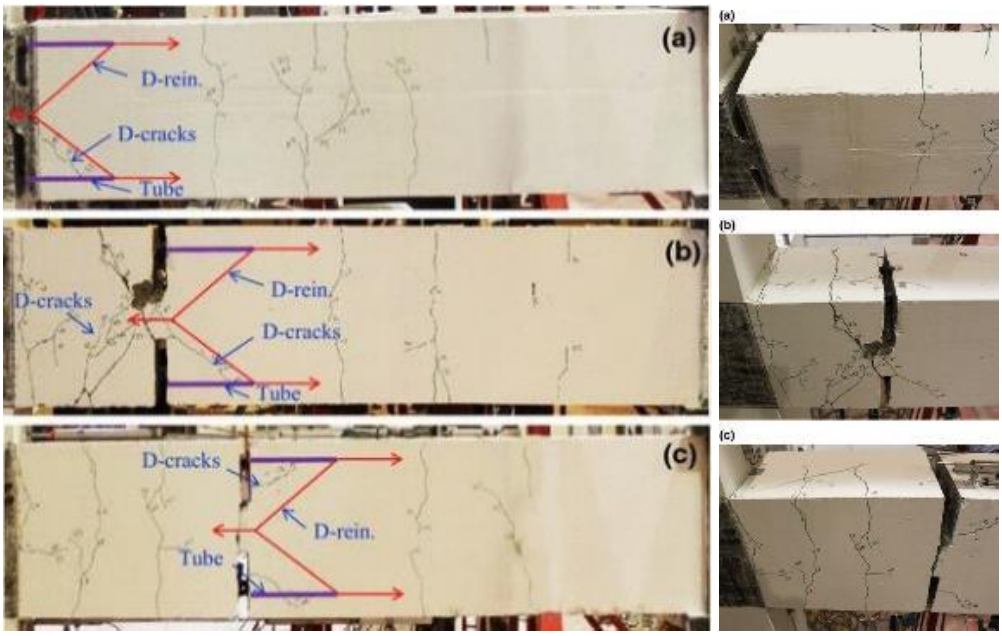

Figure 2.6: Tests of Oudah and El-Hacha specimens [26].

Pokhrel and J. Bandelt [27] conducted research in 2019 to explore the plastic hinge behaviour and rotation capacity in reinforced ductile concrete flexural elements. Through the utilization of a bond-slip constitutive model that was established not too long ago, the researchers were able to validate two-dimensional finite element models by comparing them to experimental results. Our capacity to replicate a variety of damage states, such as yield and collapse-level drift circumstances, is improved by this model. Following the completion of the validation procedure, researchers applied this modeling approach in order to explore the behaviour of plastic hinge regions in reinforced high-performance fibre-reinforced cementitious composites (HPFRCC) flexural elements. Among our primary concerns was the investigation of the several ways in which differences in geometric configurations, boundary conditions, and mechanical qualities influence performance. Key areas of interest encompassed the locations of reinforcement yielding, the distribution of plastic strain, and the regions of curvature localization. To further understanding, they proposed new expressions aimed at predicting the equivalent plastic hinge length, denoted as Lp . These expressions incorporate several influential variables, including shear span, the tensile strength of HPFRCC, reinforcement ratios, yield strength of the reinforcement, as well as the specific boundary conditions and loading scenarios encountered. This comprehensive approach not only enhances the predictive capability of the models but also contributes valuable insights into the design and assessment of reinforced HPFRCC structures under various loading conditions. The equations that have been proposed for estimating the plastic hinge length of tes HPFRCCs have been incorporated into a framework that is based on mechanics and is intended to estimate the rotational capacity of flexural components as shown in Fig 2.7. This analytical approach has shown that it is capable of approximately estimating both the yield strength and the

nominal flexural strength with a level of precision that is respectable. A comparison was made between the suggested approach and the experimental results, as well as the existing expressions for plastic hinge length that were reported in the study for both reinforced concrete and HPFRCC members. This was done in order to validate the effectiveness of the proposed technique. Under cyclic loading, Ly was longer than under monotonic loading in the majority of simulations, and strain distribution along the length of the HPFRCC external members verified this. An increase in the length of the reinforcing yielding zone, denoted by Ly, occurred when the tensile strength of the HPFRCC material declined. The length of the tensile strain concentration zone, denoted by the symbol Lsc, was shown to be shorter in simply supported beams when cyclic loading was compared to monotonic loading. However, the length of the zone was longer in cantilever beams. When simply supported beams were subjected to cyclic stress, the curvature localization zone, denoted by Lcl, was discovered to be shorter than when exposed to monotonic loading. On the other hand, the reverse situation occurred with cantilever beams.

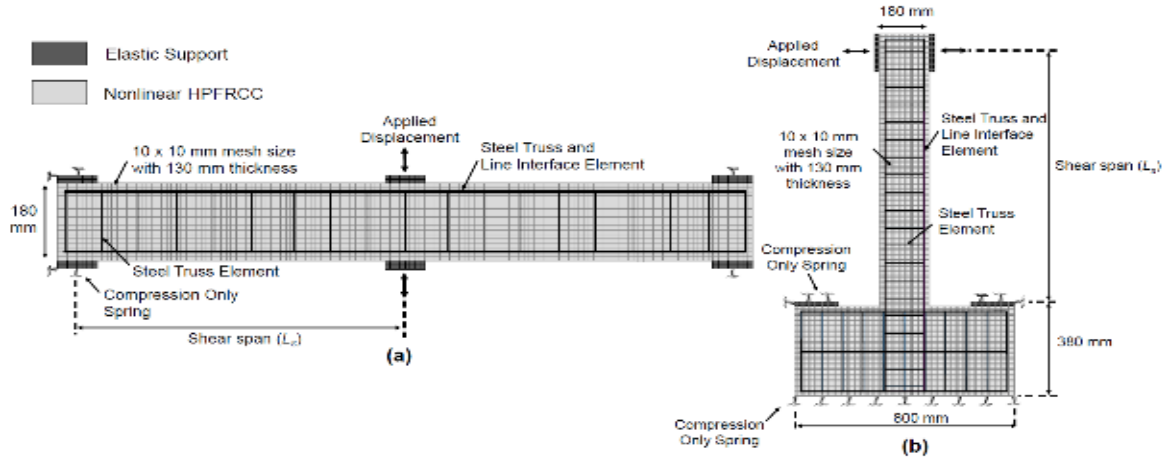

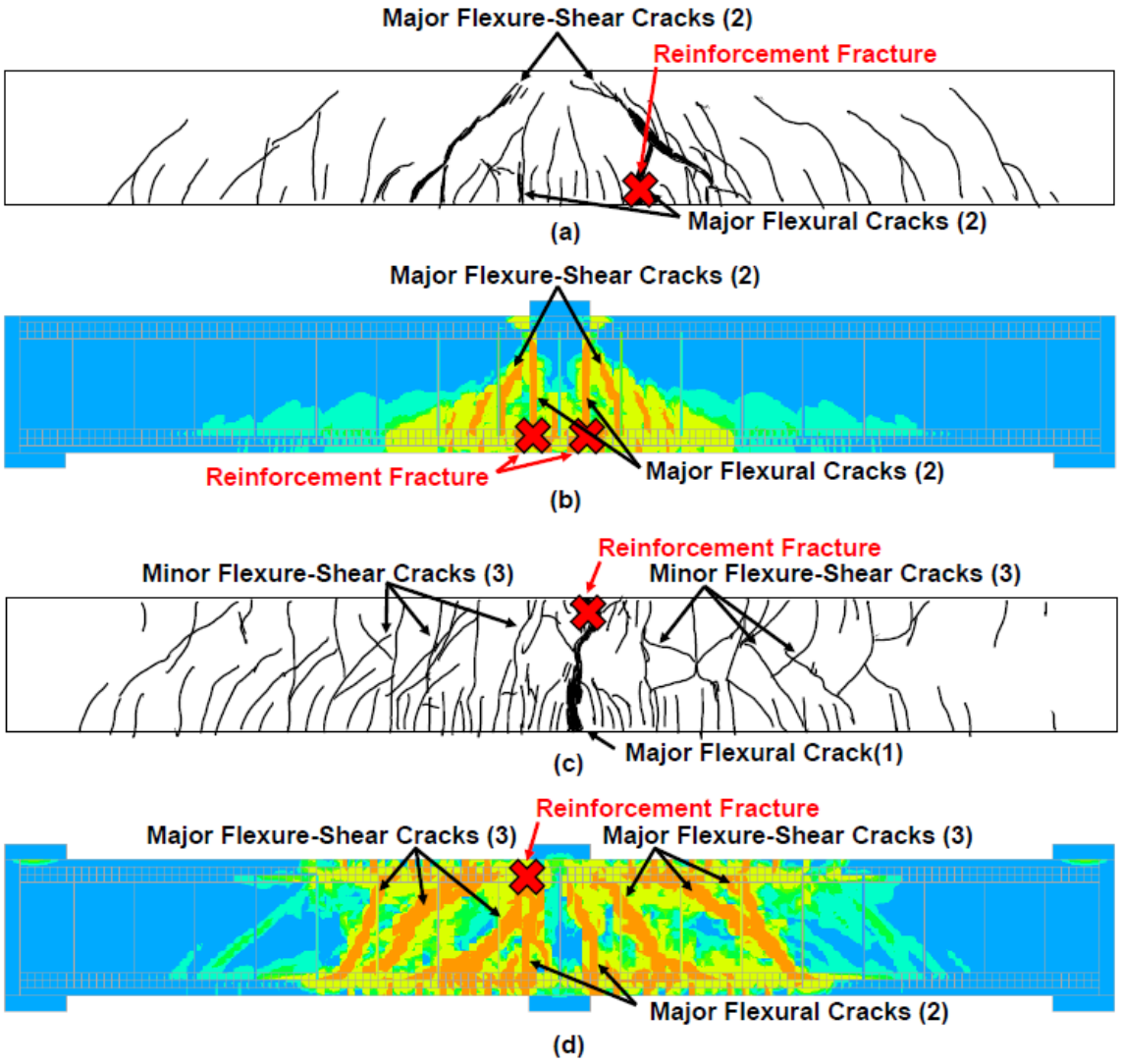

Figure 2.7: Specimens tested by Pokhrel and J. Bandelt [27]

In 2019, Farouk and Khalil [29] looked at how fexural members' plastic zones are shown. By presenting a straightforward approximation equation to calculate the plastic hinge rotation, this study attempted an analytical investigation of the topic. The proposed formula took into account a number of factors, including concrete strength, steel yield, section shape, load location, tension/compression steel ratios, and steel. Experimental data, analytical results, and hypotheses from several formulations, as well as software (ANSYS and NONLACS2), are presented and compared for simply supported beams that are exposed to moderate concentrated

loads of different properties. The essay went on to provide a mathematical model for structural analysis that could predict the beams' behaviour under deformations by using the equation that was brought up. Unlike traditional formulations, the mathematical model can predict plastic rotation and flaws all the way up to the breakdown point. The experimental results supported the projected defect levels from the mathematical model as in Fig 2.8 .

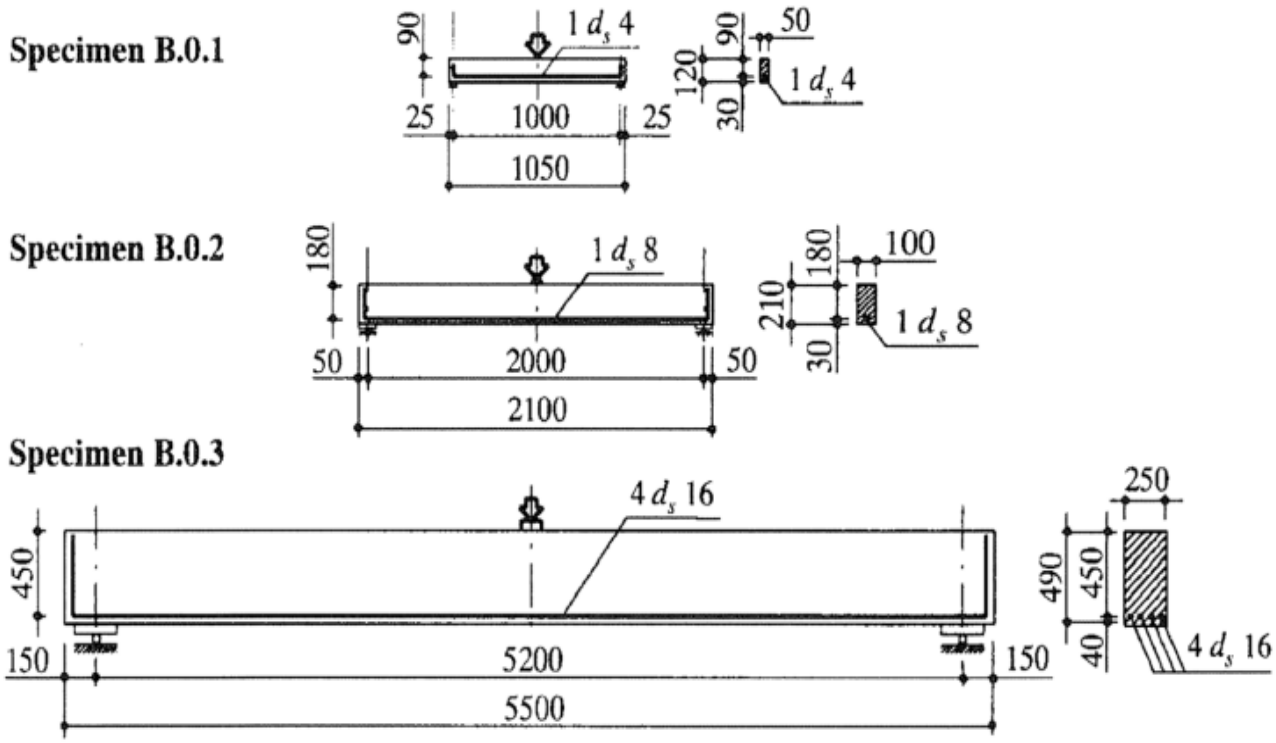

Figure 2.8: Specimens tested by Farouk and Khalil [29]

Somer (2019) [30] studied the static load failure patterns of RC beams constructed with various plastic hinge lengths. By adjusting the tension reinforcement ratio and span-to-depth ratio, this statistically validated research generated RC beams with varying failure modes as shown in Fig 2.9. In order to assure accuracy, we used a numerical model of a simply supported beam subjected to four-point loading. Instead of representing shear dominating parts as separate finite elements, the constrained concrete model was introduced to include their

effects within the concrete model. The vertical loading of all beams is controlled by displacement. Next, the beams' plastic hinge lengths were measured and compared to the findings of the preexisting equation. The results are summarised below: The stresses built up in the steel bar implanted in concrete, as well as the load-deflection relationship, may be captured using the finite element method. Beam behaviour type correlates with Lp. The control might be tension- or compression-controlled, or it can be temporary. The shear span to depth ratio value, which is referred to as thin, deep, and intermediate beam in this research, is likewise connected with Lp. For tension-controlled beams, two formulas in the literature provide identical outcomes independent of the slenderness ratio. The current research on beams constructed in compression regulated and transition zones presents very cautious estimates.

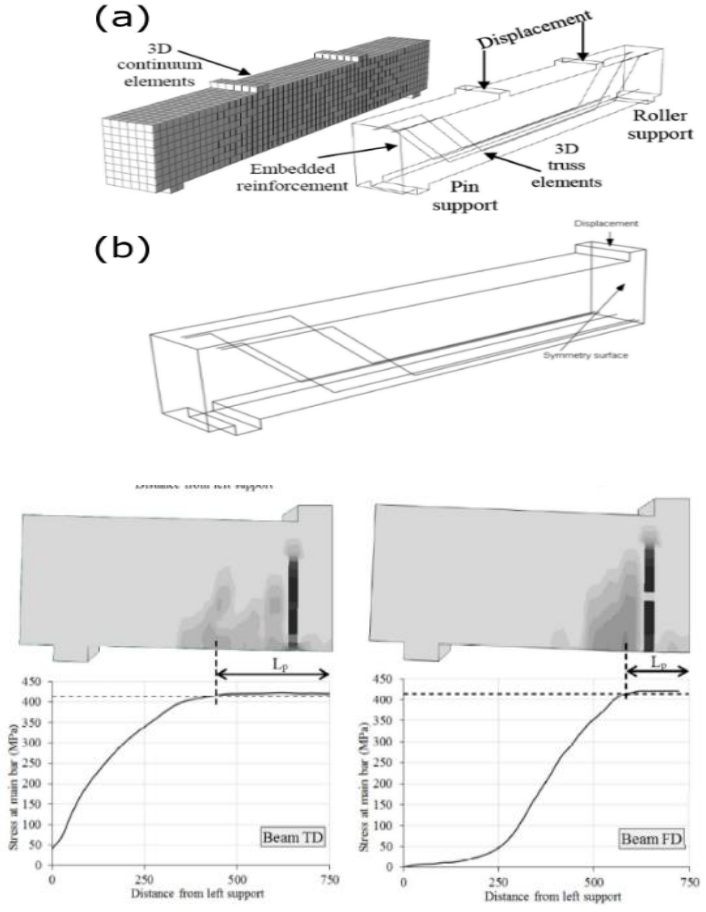

Figure 2.9: Specimens tested by Somer [30]

In 2023, Another key aspect explored was investigation the effect of different available *Lp* equations on the overall nonlinear structural response of RC frames by Sayed et al . [31] . Therefore, ten *Lp* equations were selected from this review for simulating the nonlinear behaviour of two RC frames with available experimental data. Each frame was analyzed ten times with alternative *Lp* values under pushover analysis using SAP2000 software shown in Fig 2.10 . the results of the average error in ultimate lateral load was 17.05% for the all the twenty investigations of both the studied frames. The error value is acceptable for such simple analysis. Better accuracy could be achieved by finding more reliable estimation for the *lp* based an intensive experimental plan and by considering new parameters such as the frame type whether strong or weak and the slenderness of the columns. Definitely, using a more advanced model such the distributed plasticity or full finite element analysis will improve the accuracy. 2- The average deviation in the initial lateral stiffness ranged from +20.1% to -30.4%. 3- The equation of Pauley & Priestly (1992) and the equation of Baker (1956) were the proper expressions to determine the PH length *lp* to match the real initial stiffness of RC frame; minimum deviations of +0.4% and -0.7% was recorded for the two equations, respectively. Comparing the results with Bae & Bayrak [11] and EC8 equations revealed that Bae & Bayrak [11] equations showed largest overestimation in the initial lateral stiffness of the RC frames (+20.1%). The Eurocode8 (2005) equation led to the largest underestimation in the initial lateral stiffness of the RC frames (-30.4%). Although similar parameters were used for the highlighted four equations in the previous three items, the results of these equations were different. Therefore, not only the utilized parameters but also the coefficients of these parameters govern the accuracy of a certain empirical equation. In other words, the sample used to derive the equation has direct influence on its accuracy. Increasing the plastic hinge length led to decreasing the lateral stiffness of the RC frame and vice versa. 8- Significant variation in the nonlinear

response of the RC frames was noticeable for different lp lengths based on the utilized lp equation.

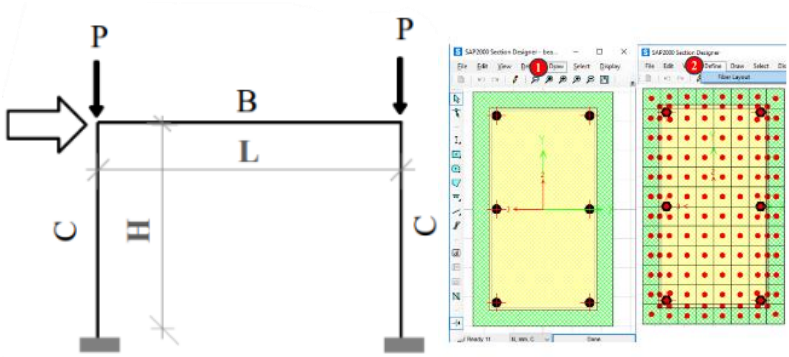

Figure 2.10: Specimens tested by Sayed et al. [31]

2.3 Enhancing techuiques of ductility in R.C. Beams

Hillerborg (1990) [21] conducted a theoretical study to analyze the stress-strain relationship in the compression zone of concrete beams. Using an approximate model incorporating localization and strain softening, the study described the descending branch of the curve as a stress-deformation relationship rather than a stress-strain one. The results indicated that the stress-strain behaviour in the compression zone was highly influenced by its depth, contradicting existing design rules that assumed no such size dependence. These theoretical findings were later validated through comparisons with experimental test results and rotational capacity measurements.

Kwan et al. (2002) [28] investigated the relationship between flexural strength and flexural ductility in beam sections. The analysis, presented in the form of charts, evaluated different concrete grades and steel reinforcement ratios. The study revealed that using higher-grade concrete could enhance flexural ductility at the same flexural strength or improve both simultaneously. Additionally, introducing

compression reinforcement without increasing tension reinforcement significantly improved ductility with only a minor increase in strength. Conversely, adding steel reinforcement in both tension and compression zones led to increases in both flexural strength and ductility.

Kwan et al. (2004) [28] investigated the influence of concrete grade and steel yield strength on the flexural ductility of reinforced concrete (RC) beams. The study expanded an existing theoretical equation linking beam section ductility to steel reinforcement ratios and concrete strength by incorporating the effects of tension and compression steel yield strengths through a parametric analysis.

The findings revealed that, for a given under- or over-reinforced beam section, flexural ductility decreased slightly with higher tension steel yield strength and concrete strength but increased marginally with higher compression steel yield strength. Charts illustrating the relationship between achievable flexural ductility and flexural strength demonstrated that using higher-strength concrete could enhance either ductility, strength, or both.

Additionally, at a constant flexural strength, increasing the compression steel yield strength improved ductility, whereas higher tension steel yield strength reduced it. Based on these results, the study proposed a simplified design method to meet specific flexural ductility requirements in beam sections.

In 2019 Jassim Kadhem[32] submitted a study that was the main aim of study is to investigate the efficiency of considering in plane non-prismatic flanges on upgrading strength rating, flexural ductility, rotation capacity without significant effect upon ultimate load capacities, stiffness, and load deflection behaviour. The main parameters experimented in this investigation were, 1- flange tapered thickness variation, 2- web thickness. Since the flexural strength is proportional to the distance

from the middle of the beam, so the non-prismatic flange was chased to this aim and the web to compared with rectangular and Tee beams. The results confirmed upgrading strength rating, flexural ductility, and rotation capacity without significant effect upon ultimate load capacities, stiffness, and load deflection behaviour. The ultimate load ratio for non-prismatic flanged in respect to rectangular beam was greater than rectangular, large ratio indicated is 1.075, this study confirming that changing section maintains ultimate strength with slightly increment, the strength rating of non-prismatic flanged section developed higher strength rating, flexural ductility and plastic sustainability higher than corresponding with control rectangular and ordinary T- beams although all had constant steel ratio and same concrete grade, the deflection curve lines at ultimate loading level have significant different and flexural ductility increased in the three group of non prismatic flanged beam, this observation enhancing that non-prismatic flanged efficiency to upgrade ductility thorough out non-prismatic flanged flexural element length, the steel reinforcement yield and flexural bending maintained with gradually spreading of cracks companied with plastic behaviour till failure occurring, plastic rotation capacity (θ) values have increased significantly for the non prismatic flanged beam compared with control beams.

2.4 Concluding Remarks

Previous studies focus on enhancing the ability of structurally reinforced concrete elements to undergo plastic deformation and so improve ration capacity without significant loss of strength. The explorers factor affecting rotation capacity, such as material properties and steel reinforcement details. In this study, a new trend of steel reinforcement details is introduced and investigated experimentally in order to assess its efficiency in ductility and section rotation capacity enhancement.

CHAPTER THREE: EXPERIMENTAL PROGRAM

3.1 General

The materials utilized, as well as the specimens cast and tested, were carried out in laboratory testing at the University of Misan. As part of the experimental effort, 14 RC beams made of regular concrete were tested. The flexural behaviour of reinforced concrete beams with aligned steel reinforcement was the primary focus of the specimens. Table (3-1) displayed the primary parameters that were taken into consideration.

Table 3-1: Used parameters.

Sq.	Beam Variables	Details
1	Curved longitudinal reinforcement	Curved steel reinforcement is used with profile options
2	Number of curved rebar	Number of used Curved longitudinal reinforcing
3	Aligned reinforcement layer	Alignment of top or bottom rebar layers in tensile side
4	Compressive strength of concrete	Using multiple values of compressive strengths

3.2 Testing Program

After deciding on a list of potential building materials, the first step is to evaluate them chemically and physically. You can enter the amount and ratio of each material, including additives, which assists in finding the best and most appropriate proportions for the concrete mixtures. To find out the mixes' mechanical characteristics, the second step is to test experimental models. And then the casting and testing of beams continues till they break. The beams' structural performance and strength characteristics can be thoroughly evaluated in this way.

3.3 Materials

The sample selection, encompassing amount, kind, and quality, was conducted with precision based on a comprehensive investigation. The meticulous selecting process occurred prior to the casting of concrete beams. The materials used in this study were commercially available and included cement, natural aggregates, natural sand, water, and a superplasticizer. These selected materials aimed to accurately represent real-world construction scenarios, ensuring the validity and relevance of the study's findings. By choosing commonly used components, the research sought to enhance its applicability in practical engineering contexts, providing valuable insights that could inform future design and construction practices.

3.3.1 Cement

The Portland cement was the main material used in this trial. At Misan University, the materials were evaluated. The cement was carefully moved and kept in a dry, temperate environment so that its properties would remain intact. Data from the specific tests are shown in Tables 3.2 and 3.3. The results were in line with the Iraqi standard 5/1984 [33], and the tests were carried out according to the ASTM C191 standard [34]. Laboratory experiments were crucial in determining the suitability and quality of cement for this investigation, which ultimately led to its selection as a material.

Table (3-2): Physical properties of ordinary Portland cement [33].

Physical Properties	Test Results	Limit of Iraqi specification
Vicat time of Setting Early: Ultimate:	 2 hr < 4	 >45 <10
strength of mortars 3-day (Mpa) 7-day (Mpa) 28-day (Mpa)	 21 28 35	 ≥ 15 ≥ 23

Table (3-3): Chemical composition of cement [33].

Compound Composite	Weight	No.5/1984Limits
Limes(Cao)	64%	N-A
Silicas(Sio_2)	21%	N-A
Alumina's(Al_2O_3)	4.6%	N-A
Iron oxidizes(Fe_2O_3)	3.3%	N-A
Magnesians(MgO)	2.4%	≤5%
Sulphates(SO_3)	2.3%	≤2.8%
Ignitions	3.6%	≤4%
Insoluble residuals(I.R.)	1.2%	≤1.5%
Limes fullness issue(L.S.I.)	0.750%	(0.66-1.02)%
T. silicates(C_3S)	50.7%	N-A
D. silicates(C_2S)	18.3%	N-A
T. aluminates(C_3A)	8.1%	N-A
Tetracalcivm aluminoferrites (C_4AF)	9.9%	N-A

3.3.2 Aggregate

A. Fine aggregate (Sand):

The Al-Zubair region in Basrah was chosen for its accessibility and significance to the study's geographical context. The sieve analysis test was conducted in accordance with ASTM C-136 [35] to assess the distribution of particle sizes in the sand. To determine the range of particle sizes in a sample, this test technique involves putting the sand through a set of sieves with progressively finer mesh sizes. Sieve analysis is useful for figuring out the sand's gradation and whether or not it's suitable for use in concrete. Figure 3.1, tables 3.4 and 3.5, and the study's standard concrete sand grading are all displayed there. The tables below give specifics regarding the percentages of different particle sizes in the sand sample. It should be mentioned that the sand utilized in this study is in accordance with Iraqi Specifications No. 45/1984 [33], meaning it satisfies the criteria set forth by the Iraqi standard.

Table (3-4): Grading the fine aggregate.

	Size of sieves (mm)	% Passing percentages	
		Fine aggregates	No.5/1984Limits (2^{th} region)
1	10	100	100
2	4.75	99	90-100
3	2.36	90	75-100
4	1.18	75	55-90
5	0.60	53	35-59
6	0.30	17	8-30
7	0.15	2	0-10

Table (3-5): Physical Characteristics of Fine Aggregate.

Physical Properties	Tests	No.5/1984Limits
Specific gravities	2.65	-
SO3	0.33	≤0.5
Preoccupation %	1.10	-
bulk density Slack (Kg/m^3)	1600	-

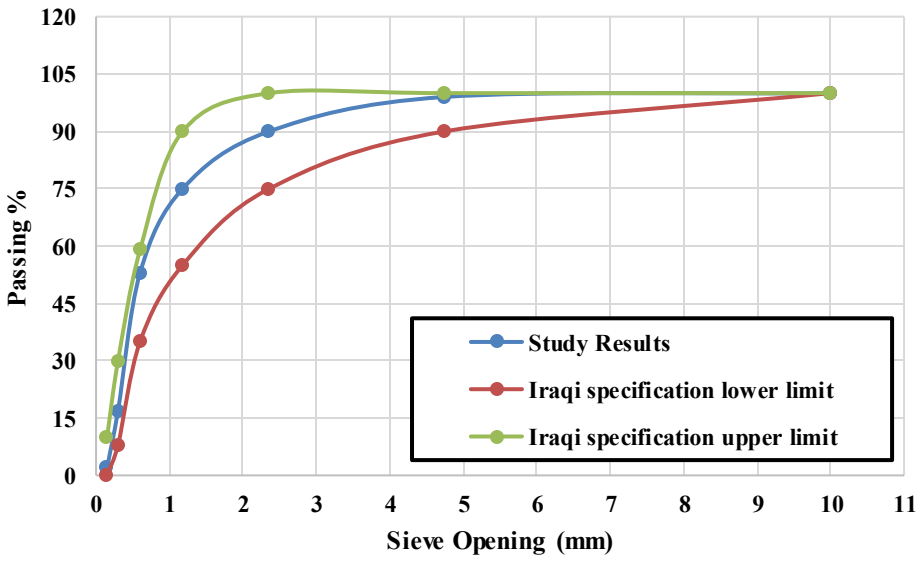

Figure 3.1 : Particle size distribution graph of fine aggregate.

B. Coarse aggregate (Gravel):

The concrete mix utilized for this experiment includes crushed gravel. Table 3.6 and Fig. 3.2 show that the crushed gravel's grading was chosen with care to meet the standards of Iraqi Specification No. 45/1984 [33] for graded gravel. The gravel will be suitable for usage in building projects if it satisfies this condition. The crushed gravel's particle size distribution was evaluated using a sieve analysis test, in accordance with the rules set out by ASTM C136 [35]. The gravel is subjected to a series of sieves with different mesh sizes to separate and determine the particle sizes in the sample. The results of the sieve test are essential for ensuring that the crushed gravel meets the required grading standards. The researchers ensured that the crushed gravel used in the concrete mix complied with Iraqi standards by conducting the sieve analysis test. This gave the study exactly what it needed. Reliability and correctness of the study outputs are enhanced by the meticulousness with which materials are selected and tested.

Table (3-6): Grading of the coarse aggregate .

No.	Sieve size (mm)	The accumulation of passing%	In accordance with IQS 45/1984, the limits	The limit of the Iraqi standard
1	37.5	100.00	100.00	100
2	20	100.00	98.5	94-100
3	14	84.62	84	82-88
4	10	46.65	44	28-2
5	5	2.91	6	0-9

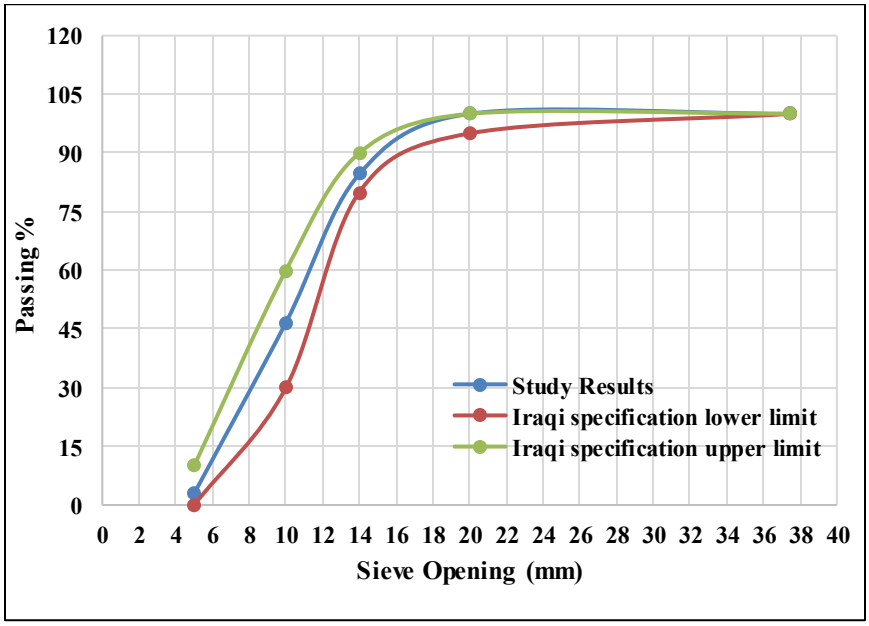

Figure 3.2: Coarse aggregate grading graph.

3.3.3 Water

R.O. water was used for both the preparation and curing of the specimens collected for this study. Water that has been purified through the process of reverse osmosis, also known as R.O. water.

3.3.4 Superplasticizer

In addition to enhancing workability and other characteristics of concrete, additives play a crucial role in determining the material's mechanical properties. Among these, water reducers are the most important additives. They significantly improve the workability of the concrete mixture, allowing it to become more workable while requiring less water. Superplasticizers, often referred to as high-range water reduction agents, are among the fastest-growing chemical additives in both the cement and concrete markets. The use of superplasticizers in the production of free-flowing concrete enabled the creation of self-compacting concrete with the required workability and resistance to segregation. Table 3.7 provides an overview of the properties and results of the tests conducted on Sika ® visco Crete 905-s [36].

Table (3-7): Types, appearances and relative density of superplasticizers.

Super-plasticizer	Chloride content	density	color
Sika ® visco Crete 905-s	NIL	1.095 kg/L	Light brownish liquid

3.3.5 Steel Reinforcement

For the purpose of this investigation, steel reinforcing rebar was utilized in the concrete specimens in many capacities, including transverse and longitudinal reinforcement. The rebar that was utilized was of one size, namely Ø8 mm, which corresponded to their constant diameters.

Table (3-8): Steel rebars properties .

Bar size (mm)	Test results		
	Yield stress (N/mm^2)	Ultimate Strength (N/mm^2)	Elongation (%)
8	441	551	18.1

3.4 Mix design and mixing procedure for concrete

Regarding the mix design, making a normal and high strength concrete mixture need more treating to fabricate a concrete beam which many trials of mixing are necessary to perform a correct concrete mix. More than one mixture was used. In order to mix the concrete, a horizontal rotary mixer was utilized. The mixing of concrete is carried out in a series of stages, the first of which involves the addition of cement, followed by the addition of aggregates. After that, various amounts of water and superplasticizer were added to the mixture in that order. In order to prevent the formation of conglomerates in the mixture, as well as to provide the concrete mix with improved workability and a more uniform consistency, the components are gradually and in small amounts added. It required far more time than anticipated to mix the high-strength concrete. For the purpose of achieving a more even distribution of the components of the concrete, particularly the aggregates, it is necessary to take into consideration a process that involves the rapid mixing of the components. Casting a cylinder with dimensions of (150x300) millimeters was done in order to conduct the splitting test. A 150x150x150 mm cube mould was utilized for the purpose of conducting compressive strength tests. A presentation of the trial mixes can be found in Tables (3-9). In the twenty-four hours that followed the casting process, the concrete was extracted from the moulds and placed in the curing conditions until it reached the age of twenty-eight days.

Table (3-9): "Ratios used in concrete mixes".

I. D	Symbol of concrete	Cement (kg/m^3)	Sand (kg/m^3)	Gravel (kg/m3)	W/C	SP (kg/m^3)	F_{cu}(MPa) in 28 days
1	C30	400	680	1108	0.54	_	30
2	C45	480	635	1082	0.381	3.26	45
3	C60	490	570	1110	0.3	3.89	60

3.5 Fresh Concrete Tests

3.5.1 Slump Test

A test that is used to determine whether or not fresh concrete is workable and whether or not it is consistent. Recording the slump measurement and interpreting the results based on the intended workability for the particular concrete mix is the final step [38]. The findings of the slump test are presented in the table and figure that can be found to the right.

Table 3.10 Results of the Concrete Slump Test

Mix No.	Target Concrete Strength (MPa) in 28 Days	Slump Value (mm)
1	30	115
2	45	100
3	60	95

Figure 3.3: Slump test of fresh concrete.

3.6 Hardening Test

Moulds are used to cast the bulk of specimens within the laboratory for the purpose of conducting hardened state tests. Following the casting process, the specimens are allowed to remain in the moulds for a predetermined amount of time, which is normally twenty-four hours. There is a period of time during which the concrete goes through the process of initial setting and early strength growth. After a period of twenty-four hours, the specimens are demolded and removed from the moulds in a safe manner. After the specimens have been moulded, they are immersed in water for the required curing length until they reach the desired testing age. This occurs in order to guarantee that the specimens have properly cured and developed their strength. The specimens are submerged in water, often in tanks or containers, in order to maintain a constant and moist environment. This process is known as water curing. This moist curing process makes it easier for the concrete to hydrate, which in turn leads to an increase in its strength. By adhering to this curing technique, the specimens are given the opportunity to reach the necessary amount of hydration and strength growth before being put through the test in their hardened state.

3.6.1 Tests for Concrete Properties

3.6.1.1 Compressive Strength Test

For the purpose of determining the compressive strength, C30,C45 and C60 cubes measuring 150 millimeters by 150 millimeters by 150 millimeters were casted. All of the specimens are held in the water basin for the duration of the complete hardening time, which is twenty-eight days, using an ELE universal testing machine that has a capacity of two hundred tons. In accordance with the information presented in Table 3-11, the compressive strength of concrete was evaluated using

three specimens for each mixture in compliance with BS1881: Part 16: 1983(BS 1881, 1989) standards[41].

Table (3-11): Evaluation of the *fcu* after 28 days.

	Compressive strength (MPa)		
Age	C30	C45	C60
7 days	22.6	30.668	41.7
	25.927	30.353	42.9
	25.286	33.54	44.9
Average of 7 days	24.457	31.5	43.167
28 days	32.4	40.5	61.6
	30.5	40.8	59.9
	29.7	39.8	61.3
Average of 28 days	30.87	40.4	61

3.6.1.2 Splitting Tensile Strength

A cylinder (150 x 300) mm was cast and test to investigate the tensile strength capacity. These tests were performed according to the specification of ASTM C496 [39]. As shown in Fig. (3.4) and Table 3.12, longitudinal crack. Three cylindrical specimens were casted and put through a series of tests for each replacement ratio as part of the examination into the tensile strength capacity potential. A diameter of 150 millimetres and a height of 300 millimetres were the dimensions of each individual cylinder. In order to carry out the tensile strength test, these dimensions are in accordance with the specifications that have been given. The testing technique was carried out in accordance with the standards that were described in the ASTM C496 specification [39]. The ASTM C496 [39] standard provides standardized procedures for measuring the tensile strength of concrete. These protocols can be used to measure the tensile strength of concrete cylinders by employing a splitting

tensile test method with concrete. An application of tensile stress was made to the cylindrical specimens while the test was being conducted. Because of this tension, the cylinders developed a crack that ran in a longitudinal direction. The cylinder experienced a significant splitting or separation along the plane of the crack, which was directly caused by the tensile stress applied to it. This phenomenon is clearly depicted in Figure 3.4, which illustrates both the longitudinal break and the subsequent splitting that occurred in the cylinder as a result of this stress. By examining this visual representation, one can gain deeper insights into the failure mode of the specimen, as well as the specific effects of the tensile stress that led to its eventual fracture. The image serves as an effective tool for understanding not only the mechanics of the failure but also the critical stress levels at which such separations occur in materials under tension.

Figure 3.4: Test of splitting tensile strength.

Table (3-12): Evaluation of the Splitting Tensile Strength.

	f_t (MPa)		
Age	C30	C45	C60
7 days	2.3	2.2	3.1
	2.1	2.5	3.4
	2.15	2.4	3.3
Average of 7 days	2.18	2.36	3.2
28 days	2.4	2.6	3.5
	2.1	2.9	3.8
	2.7	3.1	4.0
Average of 28 days	2.4	2.86	3.7

3.6.1.3 Flexural Strength

The results obtained from testing the prisms were instrumental in the investigation aimed at determining the flexural strength of the concrete specimens at various replacement ratios.. After a period of 28 days, the prism specimen received its fabrication and testing. The flexural tests were carried out in accordance with the American specification known as ASTM C78 [40].

Table 3.13 Flexural strength result

	Flexural strength (MPa)		
Age	C30	C45	C60
7 days	5.51	6.54	7.1
	4.90	6.78	7.43
	5.20	5.6	6.72
Average of 7 days	5.20	6.427	6.987
28 days	8.2	10.3	12.7
	7.6	9.7	11.5
	8.15	10.4	12.1
Average of 28 days	7.98	10.13	12.1

Figure 3.5: Flexural test.

3.7 Beam details

Casting and testing concrete beams were both tasks that were included in this effort, which comprised a comprehensive investigation. The experiment involved the design and fabrication of a total of fourteen beams, each of which had a number of parameters. (200 x 350 x 1850) millimeters are the dimensions of the rectangular beams that are manufactured, and they are then separated into many series. The investigation into the behaviour of flexural beams is carried out by means of two series, each of which has a separate set of variables. In the first series, the curving profile of rebar is going to be investigated, and in the second series, the straight alignment of the main rebar of the RC beams is going to be included. This is shown in Figure 3.7 and Table 3.13.

Table 3.14 Beams details.

Var.	symbol	Reinforcement Description	Dimensions (mm)			Compressive Strength (MPa)
			Width	height	Length	
Curvature along full	BCFS0	Straight reinforcement	200	350	1850	45
	BCF22	Curvature two bars above	200	350	1850	45

	BCF23	Curvature three bars above	200	350	1850	45
	BCF25	Curvature all above bars	200	350	1850	45
	BCF1222	Curvature four bars as shown	200	350	1850	45
	BCF12	Curvature two bars below	200	350	1850	45
	BCF13	Curvature three bars below	200	350	1850	45
	BCF15	Curvature all below bars	200	350	1850	45
	BCF#25	Curvature all above bars	200	350	1850	30
	BCF##25	Curvature all above bars	200	350	1850	60
Triangles along full length	BTF22	Triangles two bars above	200	350	1850	45
	BTF23	Triangles three bars above	200	350	1850	45
	BTF25	Triangles all above bars above	200	350	1850	45
	BTF1222	Triangles four bars as shown	200	350	1850	45

*$\rho = 0.007$, $\rho_{min} = 0.003$, $\rho_{max} = 0.001$

Notation

B I J M N

B: Beam

I: Shape of bars (C: curved , T: triangular)

J: Reinforced along length

M: Number of layers (1:first layer , 2:second layer)

N: Number of bars are (curved or triangular)

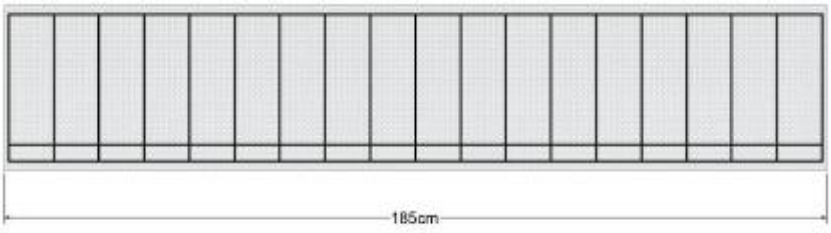

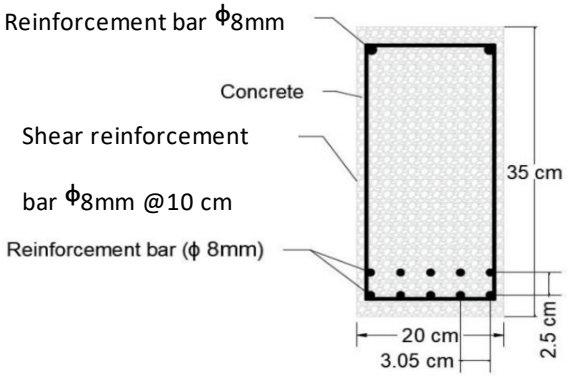

BCFS0

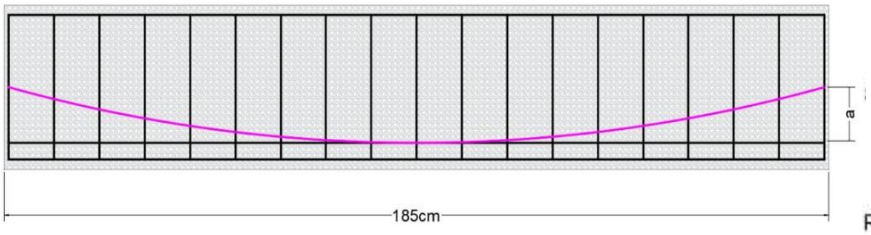

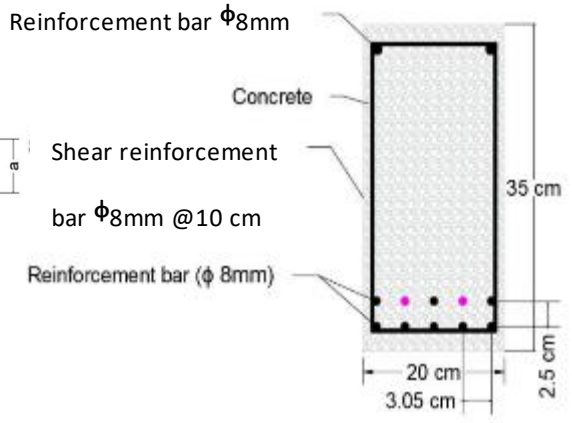

BCF22 $a = \frac{h}{2}$

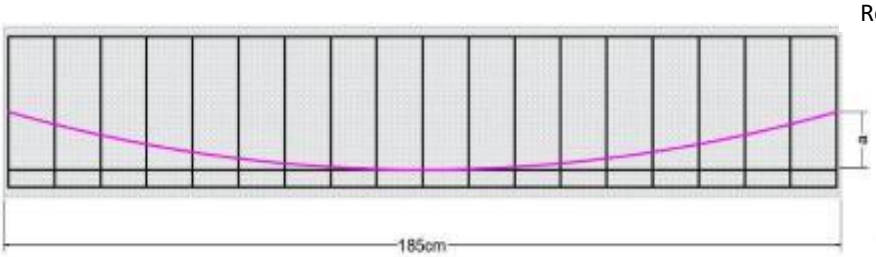

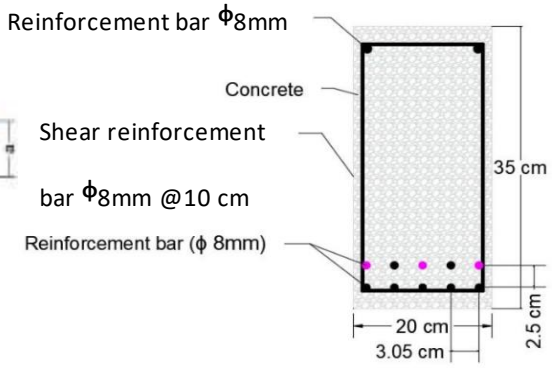

BCF23 $a = \frac{h}{2}$

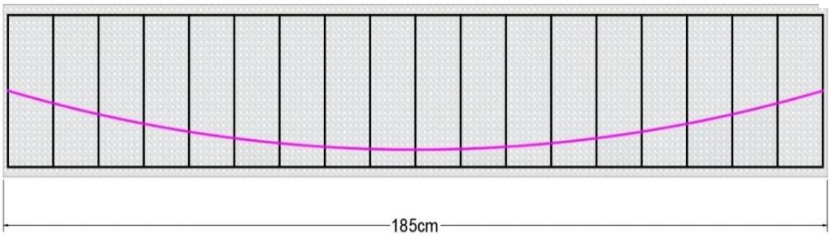

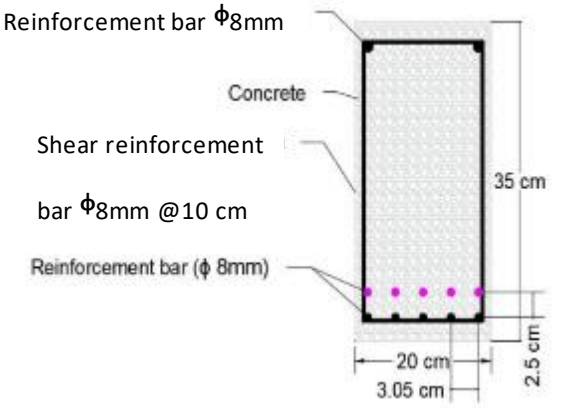

BCF25 $a = \frac{h}{2}$

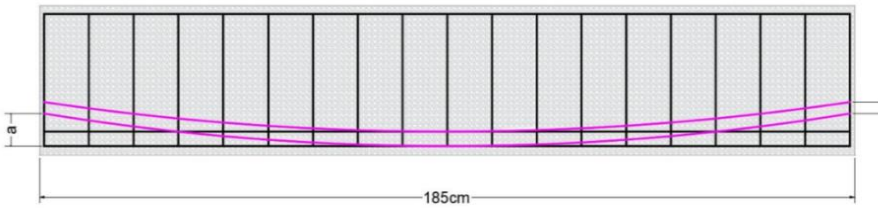

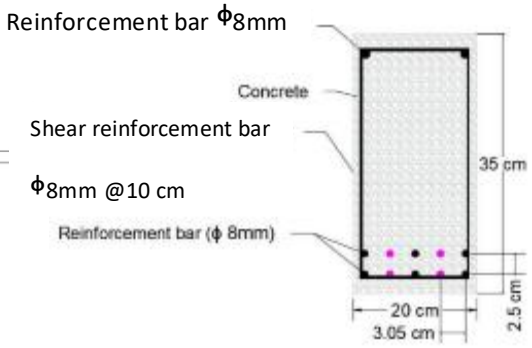

BCF1222 $a = \frac{h}{2}$

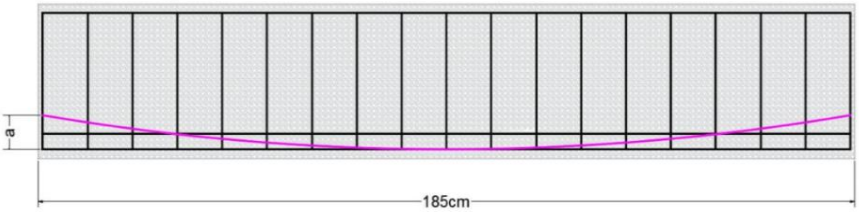

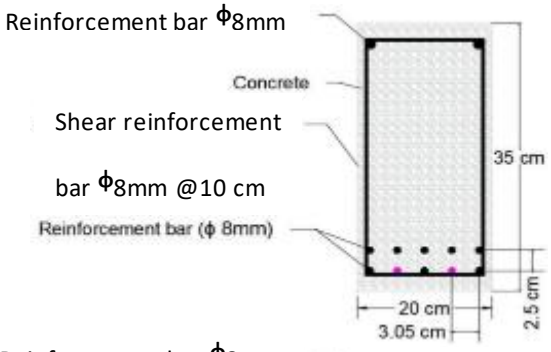

BCF12 $a = \frac{h}{2}$

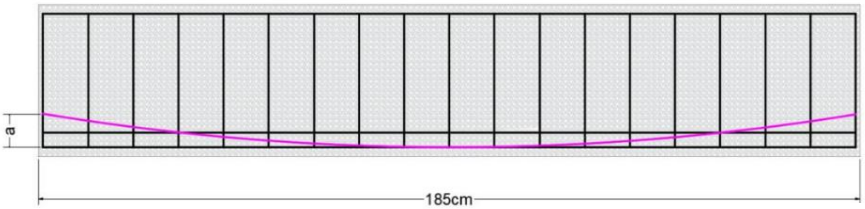

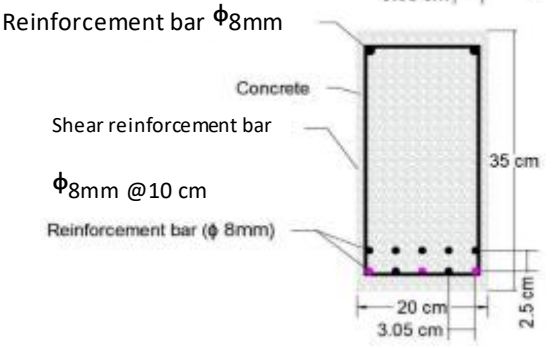

BCF13 $a = \frac{h}{2}$

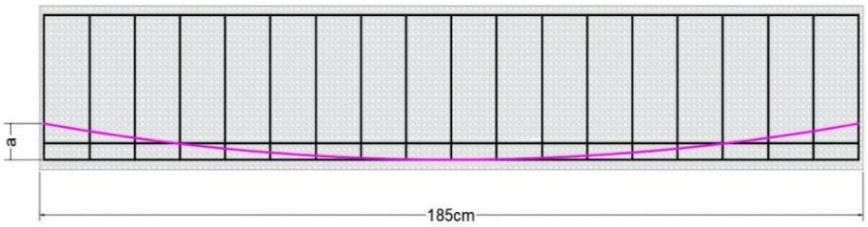

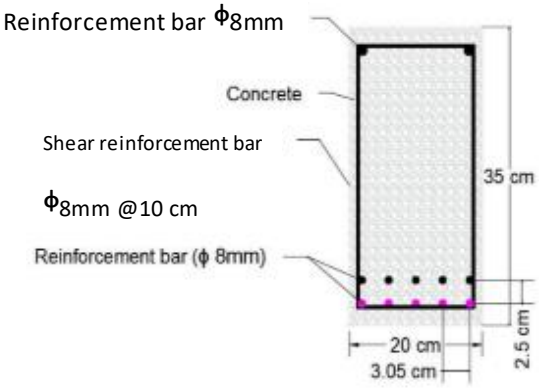

BCF15 $a = \frac{h}{2}$

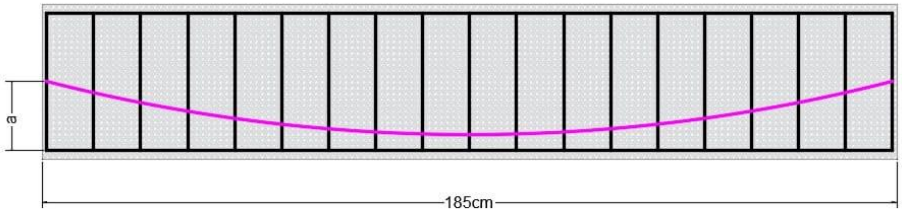

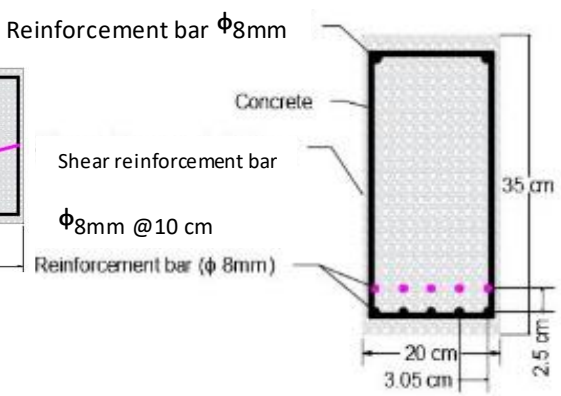

BCF#25 $a = \frac{h}{2}$

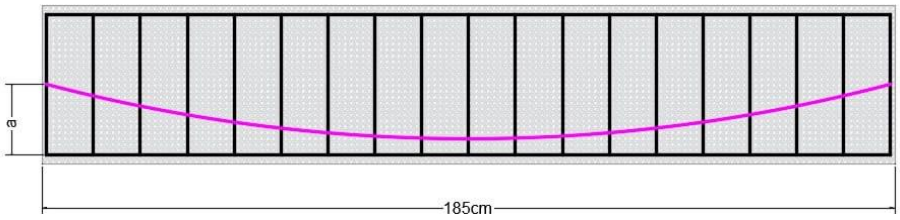

BCF##25 $a = \frac{h}{2}$

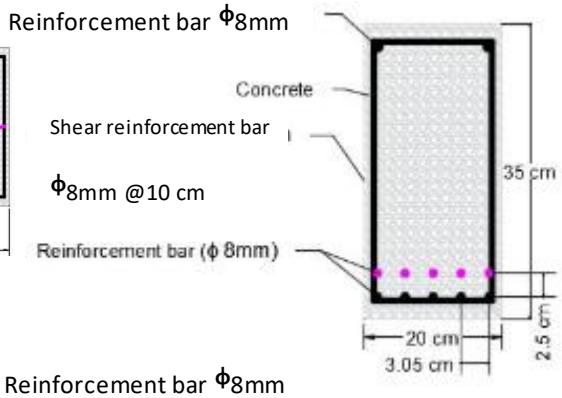

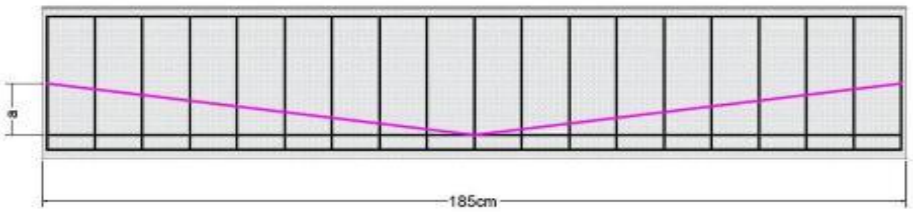

BTF22 $a = \frac{h}{2}$

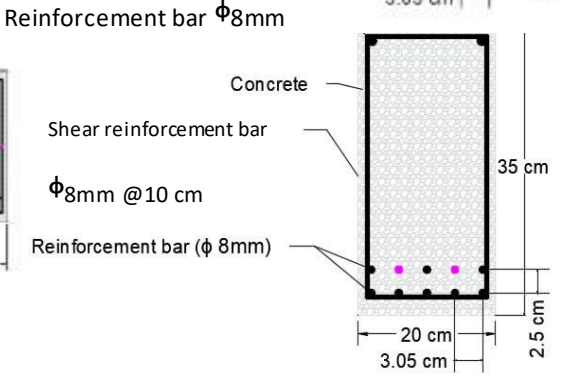

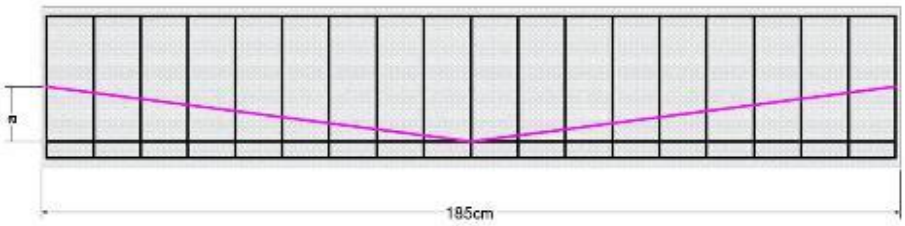

BTF23 $a = \frac{h}{2}$

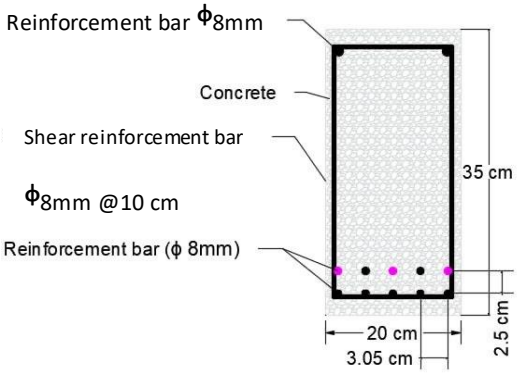

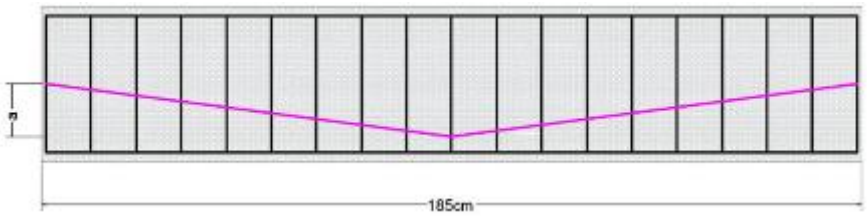

BTF25 $a = \frac{h}{2}$

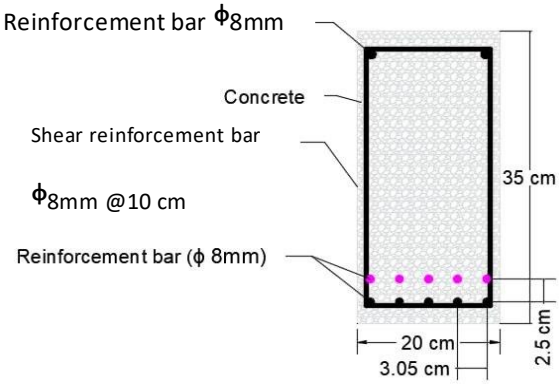

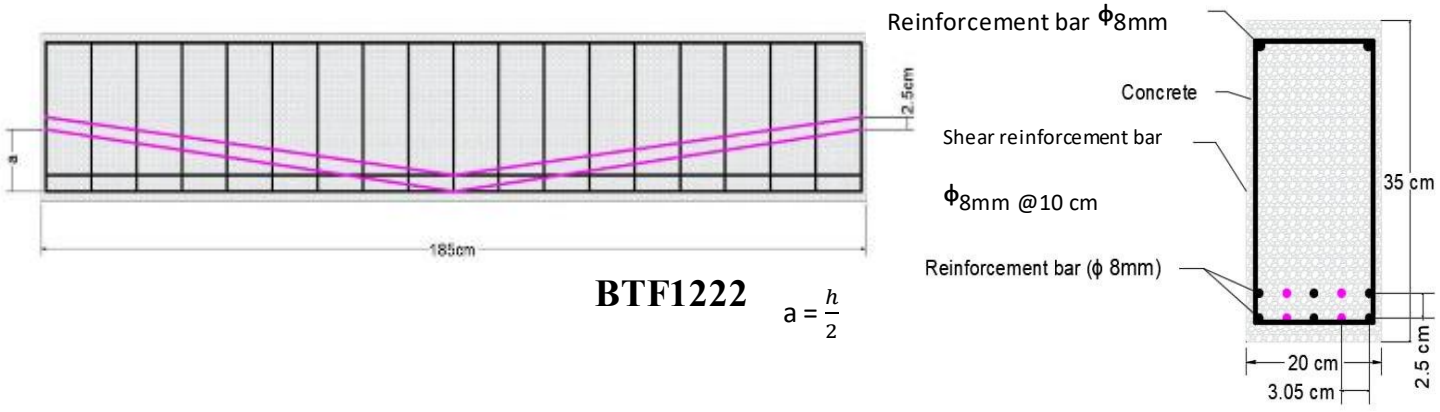

Figure 3.6: Beam details.

Figure 3.7: Details of reinforced

3.8 Mould Preparation and Casting Procedure

Prior to mould fabrication and concrete casting, the steel reinforcement cage was prepared as shown in Fig. 3.7. Fourteen plywood moulds, with dimensions matching the beams (200 × 350 × 1850 mm), were cleaned and oiled to ease demoulding. Spacers were placed to maintain correct reinforcement positioning and concrete cover. The concrete was mixed for 10–12 minutes to ensure uniformity, then poured into the moulds using vibrators for proper consolidation. The surface was levelled and smoothed, and specimens were cured.

A 100 kg mixer was used, with all materials—aggregates, cement, and water—carefully weighed and mixed in a clean container for accuracy and quality. Steel bars served as spacers inside the forms to keep reinforcement at the correct depth. Plywood forms shaped the specimens, while steel forms were used where extra support was needed.

After casting, the forms remained for 24 hours before removal. Specimens were cured in water for 28 days to ensure strength and durability. Additional cube and cylinder samples were taken to measure compressive strength, confirming the concrete met quality standards

Figure 3.8: Fabrication, moulds, and casting of the specimens.

3.9 Recording Results and Testing

A testing machine with a capacity of 600 Ton was utilized to test the fabricated beams as exhibited in Fig. 3.11. During the loading and at each load step, the loading data and strains were recorded. For the purpose of providing the optimal testing conditions and preventing the initial failure or crushing of the concrete due to the big step of loading, all of the beams were tested at the automatic loading step . It was reported that the deflection, strain, and crack width were all measured at the conclusion of each loading phase. The data acquisition system used in this setup consists of a personal computer and a strain indicator known as the data logger. The specific data logger model employed is the GEODATALOG 30-WF6016. This data logger is designed to receive data from a collection of strain gauges that are attached to the beam. The GEODATALOG 30-WF6016 is equipped with 16 channels for data obtaining, allowing the simultaneous measurement of multiple strain gauges or sensors. The data logger operates with a power supply of 110-240 V at 50-60 Hz, single-phase. The data logger comes complete with DATACOMM software, which is installed on the personal computer. This software is specifically designed for PC data obtaining systems, enabling the user to collect, monitor, and analyse the data obtained from the strain gauges.

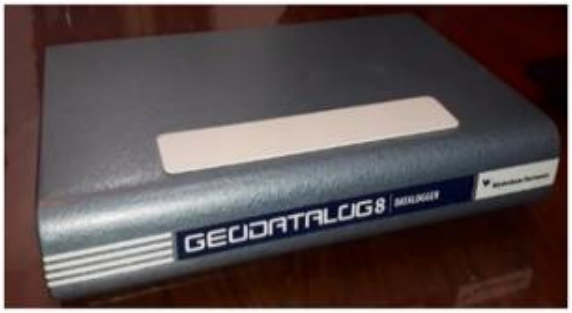

Figure 3.9: Tools used for the testing process.

Figure 3.10: Specimens before testing

Figure 3.11: Test of Specimens

CHAPTER FOUR : RESULTS AND DISCUSSIONS

4.1 General

The primary purpose of this experimental research was to contribute more information regarding the effect of steel reinforcement configurations on the ultimate strength and the mechanical properties of reinforced concrete beams. This inquiry was carried out with the primary objective of contributing more information. In general, it has been noticed that the brittleness of the concrete places a significant limitation on the steel reinforcement configurations that can be used for such elements. In spite of this, it is abundantly clear that this capacity can be expanded to a significant degree by ensuring that appropriate strength is provided in many configurations. An extensive experimental study was devoted to the evaluation of the effect of this parameter. There has been a relatively little quantity of study work done to analyse the influence of substantial reinforcement on the deformation capacity and plastic behaviour of concrete. This could be attributable to the fact that there has been so little research work done. A two central point load was applied to three sets of fourteen simply supported beams, and these beams were reinforced with variable amounts of longitudinal reinforcement utilizing multiple configurations while being subjected to the load. To investigate the impact of the primary reinforcement, this was carried out.

4.2 Overview of Experimental Results

4.2.1 Curved Aligment of Rebar / Mode I

This section presents a comprehensive summary of the experimental results obtained from testing reinforced concrete (RC) beams, focusing on findings such as cracking load, ultimate load, load-deflection curves, ductility index, stiffness, energy

absorption, and failure modes. The study involved the evaluation of RC beams with two configurations—those with aligned reinforcement and those without. Additionally, two models with differing compressive strengths were considered to further investigate the impact of reinforcement configurations on the structural behaviour of the beams. Each beam was subjected to static loads until failure, and the results are summarized in Table 4-1. The strength of the tested specimens ranged between 184 kN and 284.82 kN, while the displacement observed varied from 20.48 mm to 34.88 mm. This analysis provides critical insights into the performance of different reinforcement configurations under static loading conditions, contributing valuable data to the understanding of structural behaviour in RC beams. The variance in the ultimate load carrying capacity was due to the effect of parametric study such as the depth of reinforcing layer, in addition to the presence of curved bars. The depth of the reinforcing layer are important parameters that significantly influences the strength and displacement characteristics of the beams. By analysing the data from the tests, valuable insights can be gained regarding the curving of the reinforcing layer. The inclusion of curved bars within the reinforcement configuration plays a crucial role in enhancing the load-bearing capacity and overall structural performance of the beams. Understanding these effects allows for improved design considerations in future reinforced concrete applications.

Table 4-1:Curved Aligned steel reinforcement RC beams results

I	Beam remark	Cracking Load (kN)	Ultimate load (kN)	Ultimate Deflection (mm)	Ductility index	Energy absorption (kN.mm)	Compressive Strength Mpa	Stiffness (KN/mm)
1	BCFS0	55.27	184	20.48	3.33	1892	45	13.82
2	BCF22	58.46	205	22.72	3.51	2505.01	45	17.17

3	BCF23	61.54	231	23.36	3.75	3046.12	45	18.07
4	BCF25	59.73	243	26.2	4.07	3492.63	45	22.80
5	BCF1222	82.06	241.20	29.21	4.85	3335.83	45	24.10
6	BCF12	57.85	192.57	21.43	3.49	1980.17	45	16.99
7	BCF13	59.72	209.43	23.21	3.59	2517.54	45	17.54
8	BCF15	59.14	244.4	28.61	4.94	3068.82	45	17.37
9	BCF#25	45.97	222.4	34.88	5.2	3347.05	30	13.50
10	BCF##25	79.48	284.82	31.70	4.79	3691.03	60	23.34

4.2.1.1 Ultimate strength

In this section, the impact of steel reinforcement configuration on the behaviour of (RC) beams is presented. The introduction of curved steel rebar significantly influenced the performance characteristics of the beams, leading to improvements in cracking load, ultimate load, deflection, ductility index, and energy absorption. The control beam, which utilized straight steel reinforcement, exhibited a cracking load of 55.27 kN and an ultimate load of 184 kN. Notably, these values demonstrated significant enhancement when straight steel rebar was replaced with curved rebar. Specifically, the specimen designated as BCF12, which incorporated two curved steel rebars, exhibited an increase in cracking load of 4.7% and an enhancement in ultimate load of 4.65% in Fig 4.1. These results indicate a favorable improvement in the structural behaviour of the RC beams. Furthermore, increasing the number of curved rebars from two to three resulted in further enhancements in both cracking

and ultimate loads when compared to the control beam as in Fig 4.2. While the percentage increase in cracking load was slightly less at 8%, the ultimate load demonstrated a marked improvement of 13.8%, as illustrated in Figure 4.3 and Figure 4.4. These findings underscore the effectiveness of the curved reinforcement configuration in optimizing the performance of reinforced concrete beams.

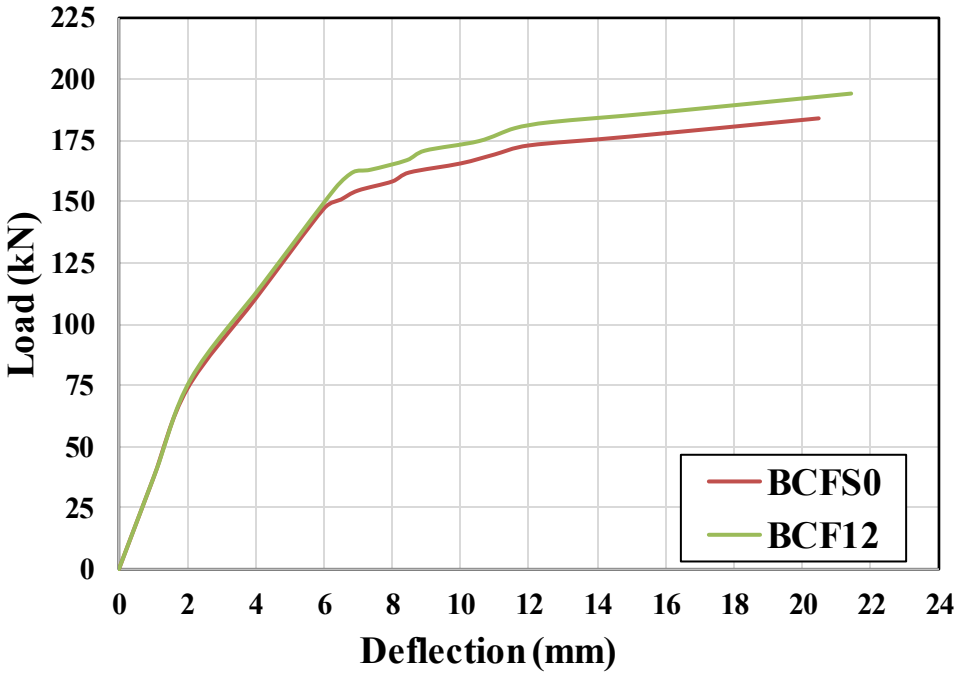

Figure 4.1 : Load deflection curve of BCF12 beam.

Increasing the number of curved rebars to five in the second layer of the bottom longitudinal reinforcement resulted in an 8% increase in cracking load. Additionally, the ultimate strength rose to 243 kN, reflecting a substantial 32% improvement. This enhancement represents the highest increase in ultimate strength, serving as an indicator of improved plastic limit behaviour for the concrete beam, all while maintaining the same reinforcement ratio . With respect to deflection, the curvature of the steel rebar led to significant increases in deflection. The introduction of two and three curved rebars resulted in icreasing to 10.9% and 16.4%, respectively, as shown in Table 4.1. The most pronounced deflection was observed

in model BCF25, which incorporated five curved rebars, yielding a 27.9% increase, as illustrated in Figures 4.5 , 4.6 and 4.7.

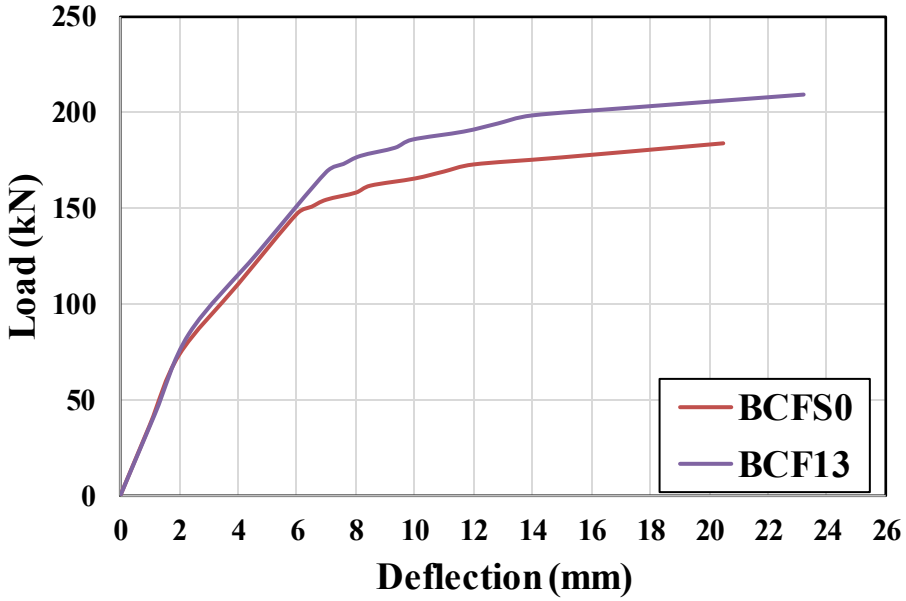

Figure 4.2: Load deflection curve of BCF13 beam.

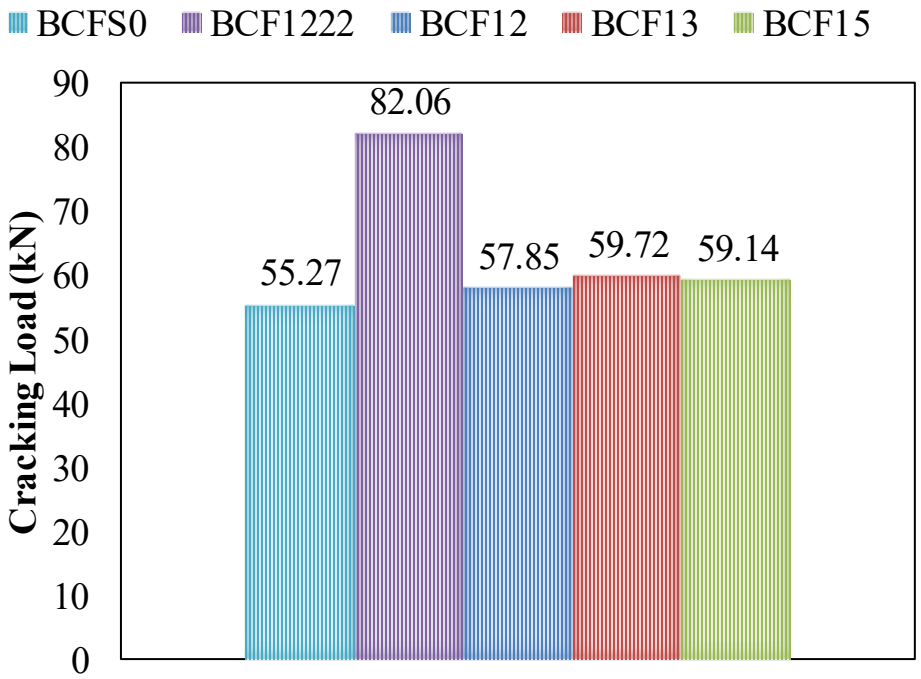

Figure 4.3: cracking load of curved steel reinforcement beams.

The results illustrate that the curving of steel reinforcement significantly influences the mechanical properties of reinforced concrete (RC) beams. The initial enhancements in both cracking load and ultimate load observed in specimen BCF22 suggest that the curved configuration improves the bond between the concrete and the reinforcement. This leads to better load distribution and an increased resistance to initial cracking. Furthermore, the increases in ultimate load with the addition of curved rebars indicate that this configuration facilitates more effective force transfer within the structure, ultimately enhancing the overall load-carrying capacity. Resulting in a more efficient load transfer mechanism. The substantial rise in both cracking load and ultimate strength with the introduction of five curved rebars signifies a shift in the failure mechanism of the beam. The curved rebar configuration appears to enable the concrete to better accommodate applied forces, thereby enhancing the plastic behaviour and ultimate capacity of the composite material Fig 4.8. However, the increase in deflection associated with the use of curved rebars suggests a potential trade-off between flexibility and load-carrying capacity. While the curved conuration improves ductility, it also leads to higher deflections, which could affect serviceability and usability. When placing curved reinforcement in both layers BCF1222, was obtained 241.20 in Fig 4.9 .

For specimen BCF#25, which featured a curved top layer of steel reinforcement with a compressive strength of 30 MPa, the observed cracking load was measured at 45.97 kN. This value is lower than that of the specimen BCF25, indicating that the compressive strength of the concrete has impacted the initial cracking behaviour.

However, the ultimate load capacity for this specimen was recorded at 222.4 kN, reflecting a 9.2% decrease compared to the specimen BCF25. This suggests that, although the initial cracking occurs at lower loads, the overall structural integrity and load-carrying capacity are enhanced due to the curvature.

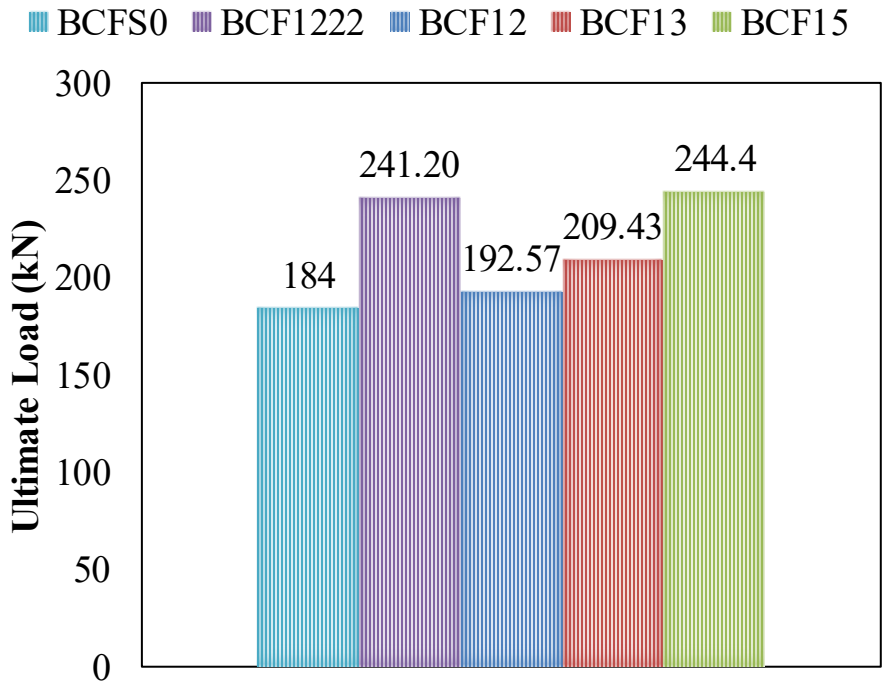

Figure 4.4: Ultimate load of curved steel reinforcement beams.

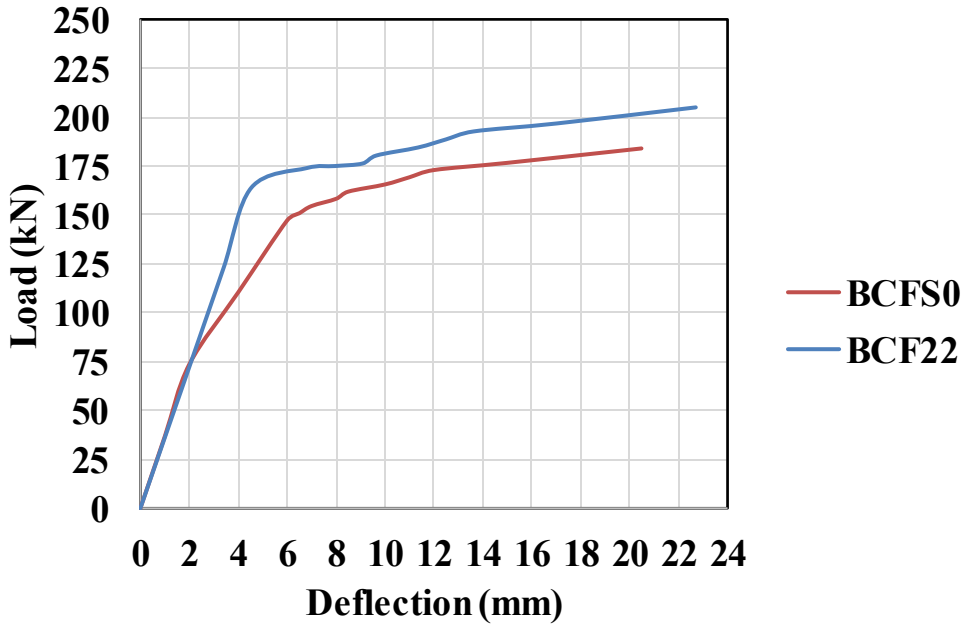

Figure 4.5: Load deflection curve of curved steel reinforcement beams.

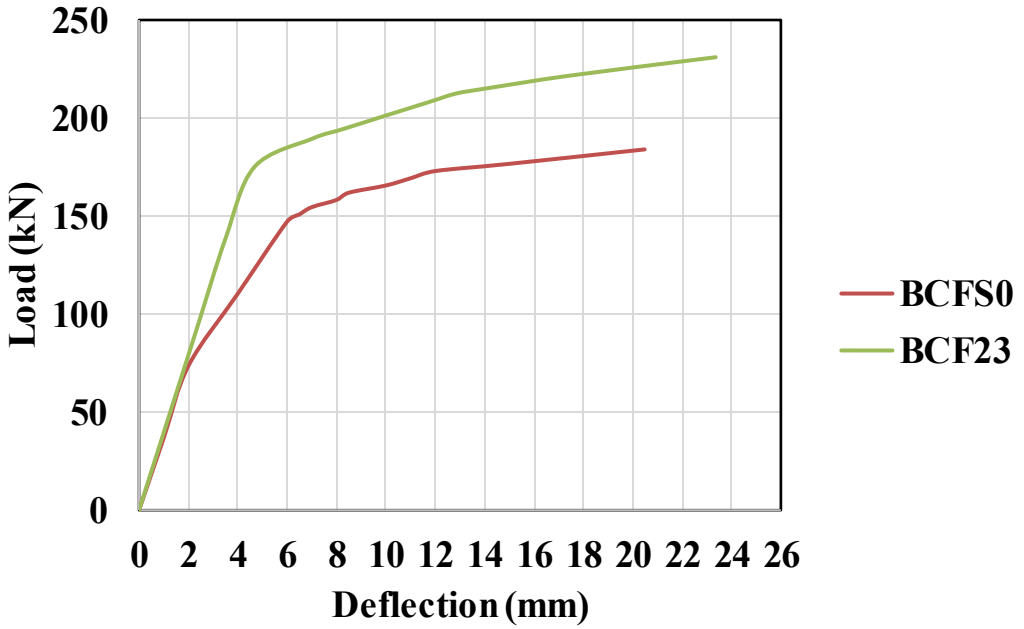

Figure 4.6: Load deflection curve of curved steel reinforcement beams

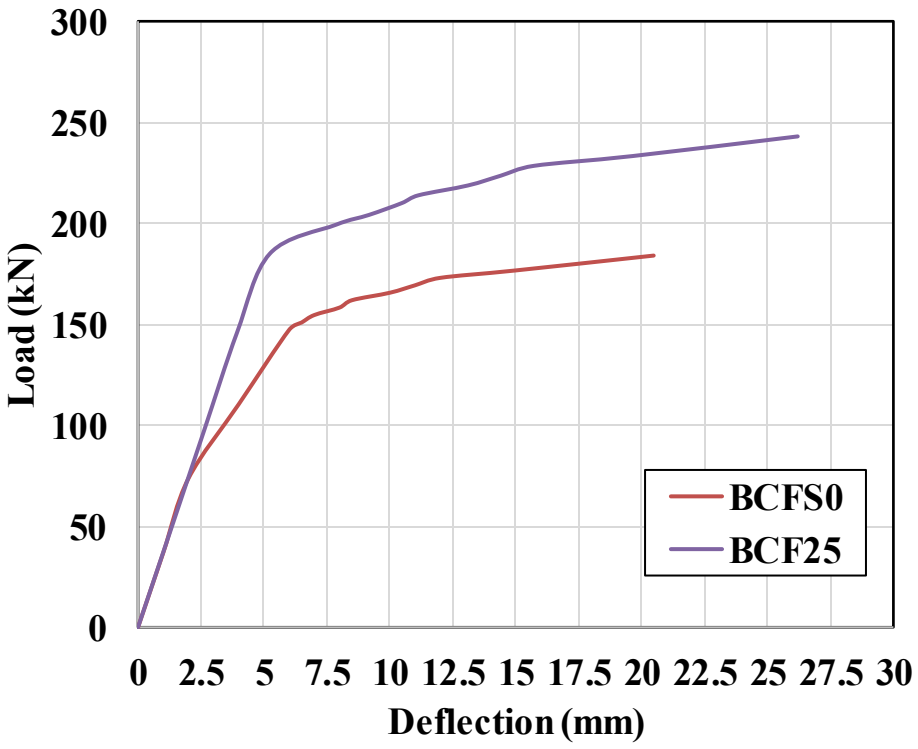

Figure 4.7: Load deflection curve of curved steel reinforcement beams.

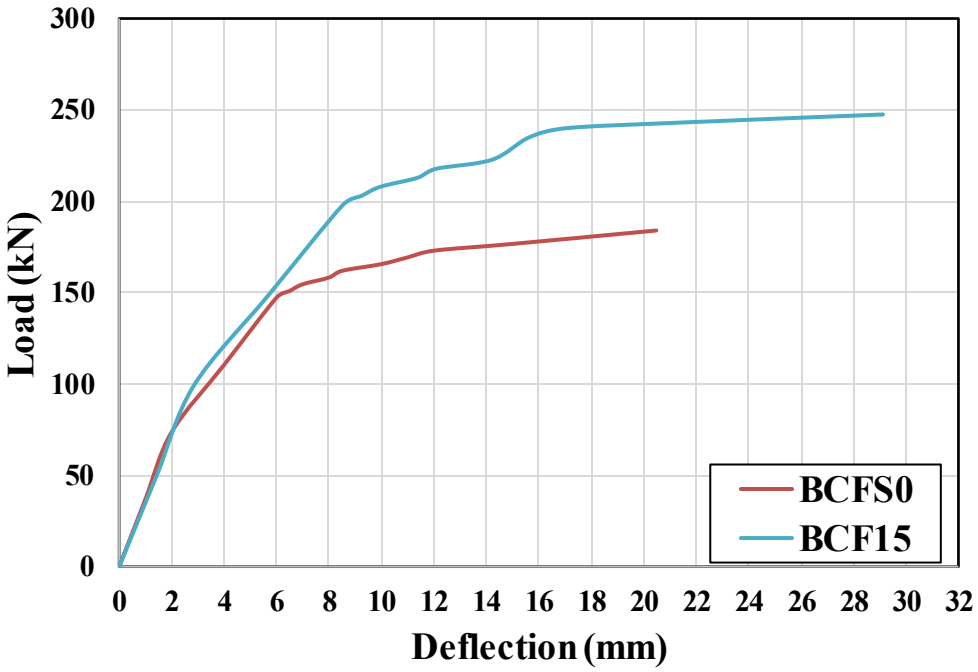

Figure 4.8: Load deflection curve of BCF15 beam.

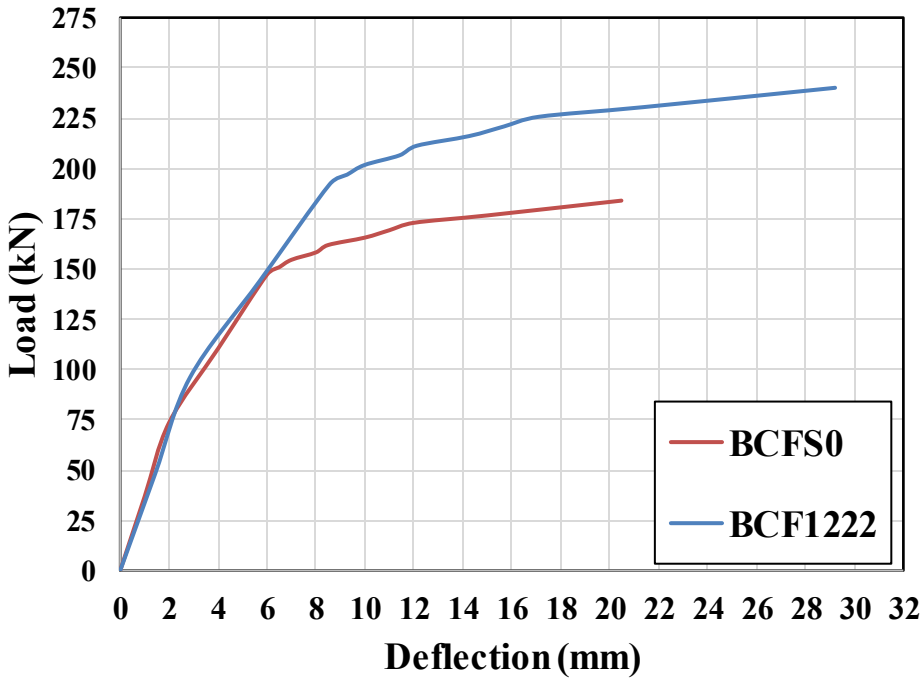

Figure 4.9: Load deflection curve of BCF1222 beam.

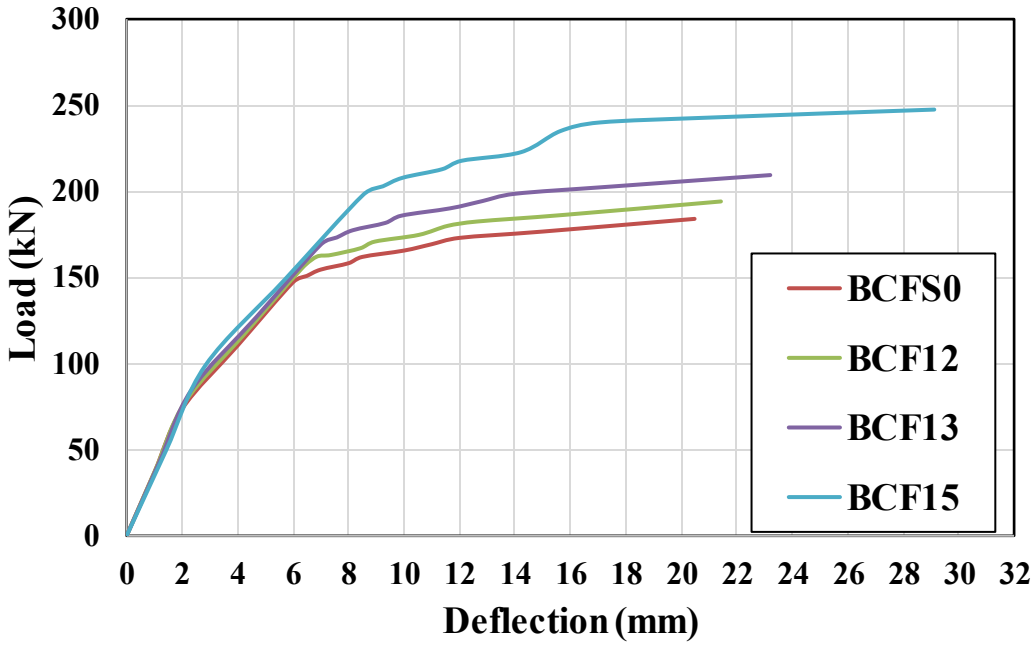

Figure 4.10: Load deflection curve of curved steel reinforcement beams with different aligned number of rebars

When the compressive strength was increased to 60 MPa, the cracking load showed significant increasing, rising to 79.5 kN. This represents a 33% increase compared to the specimen BCF25 and a remarkable 72.9% increase in comparison to specimen BCF#25, as illustrated in Figure 4.11. This indicates a positive correlation between compressive strength and the cracking behaviour, reinforcing the idea that higher material strength improves initial crack resistance. In terms of deflection, Specimen BCF#25 exhibited a deflection of 34.88 mm, which was 33.12% higher than the specimen BCF25. This suggests that the curved geometry may introduce additional flexural demands on the beam, leading to greater deflection. However, increasing the compressive strength to 60 MPa reduced the deflection to 31.70 mm, highlighting that higher compressive strength not only enhances load capacity but also reduces deflection under loading conditions as revealed in Fig. 4.12. For specimen BCF#25, which utilized a curved top layer of

steel reinforcement with a compressive strength of 30 MPa, the observed cracking load was 45.97 kN. This value is lower than that of the control beam, indicating that the introduction of curvature in the reinforcement have affected the initial cracking behaviour. However, the ultimate load capacity for this specimen was recorded at 222.4 kN, which is an increase of 20.9% compared to the reference beam. This suggests that while the initial cracking may occur at lower loads, the overall structural integrity and load-carrying capacity were enhanced due to the curvature. When the compressive strength was increased to 60 MPa, the cracking load improved significantly to 79.5 kN, representing a 72.89% increase compared to the specimen BCF#25. This indicates a positive correlation between compressive strength and the cracking behaviour, reinforcing the idea that higher material strength improves initial crack resistance. In terms of deflection, Specimen BCF#25 exhibited a deflection of 34.88 mm, which was 70.3% higher than the control specimen. This suggests that the curved geometry may introduce additional flexural demands on the beam, leading to greater deflection. However, increasing the compressive strength to 60 MPa reduced the deflection to 26.55 mm, highlighting that higher compressive strength not only enhances load capacity but also reduces deflection under loading conditions as revealed in Fig. 4.11 and 4.12. The results indicated a clear benefit from using curved rebar configurations in terms of enhancing the compressive strength and overall performance of RC beams. The initial reduction in cracking load for specimen BCF#25 can be attributed to the stress distribution and curvature effects, which may lead to an earlier onset of cracking compared to straight rebars. The curvature can concentrate stresses differently, affecting the initiation of cracks under lower loads. However, the significant increase in ultimate load capacity suggests that the curved rebar configuration effectively improves the load-carrying capability of the beams. The enhanced bond between the curved rebar and the surrounding concrete may contribute to better force transfer

and redistribution, which helps delay failure. The improvement in cracking load with increased compressive strength aligns with fundamental principles of material mechanics, where higher compressive strength materials exhibit better resistance to initial cracking. Thus, the combination of curvature and higher compressive strength appears to synergistically enhance the performance of the RC beams. Finally, the observed reduction in deflection with increased compressive strength reflects a common behaviour in structural materials: stronger materials tend to deform less under applied loads. The curvature of the rebar further influences the overall stiffness of the beam, contributing to the reduced deflection as the compressive strength increases.

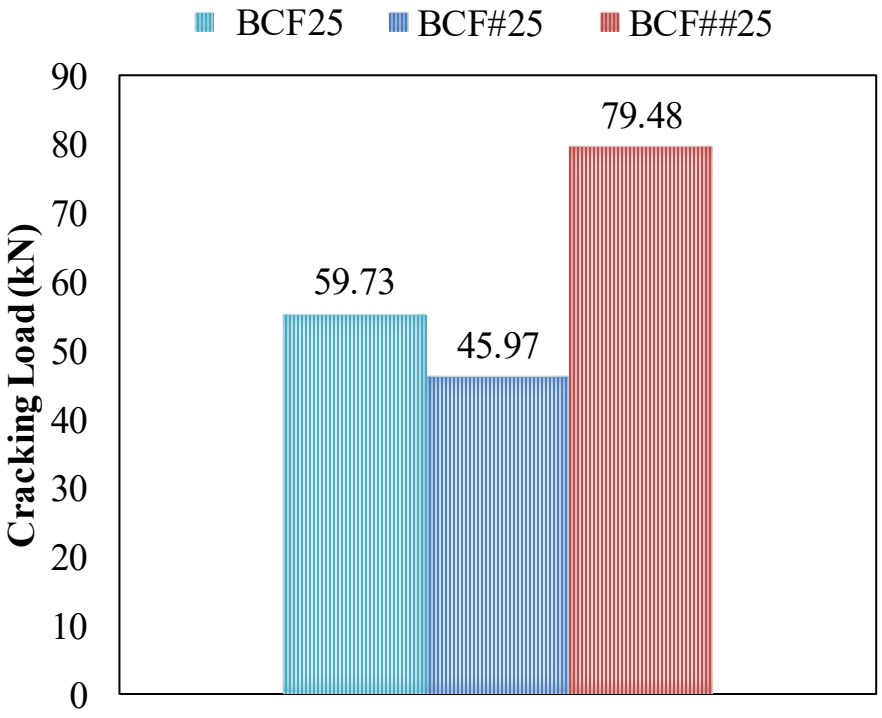

(a)

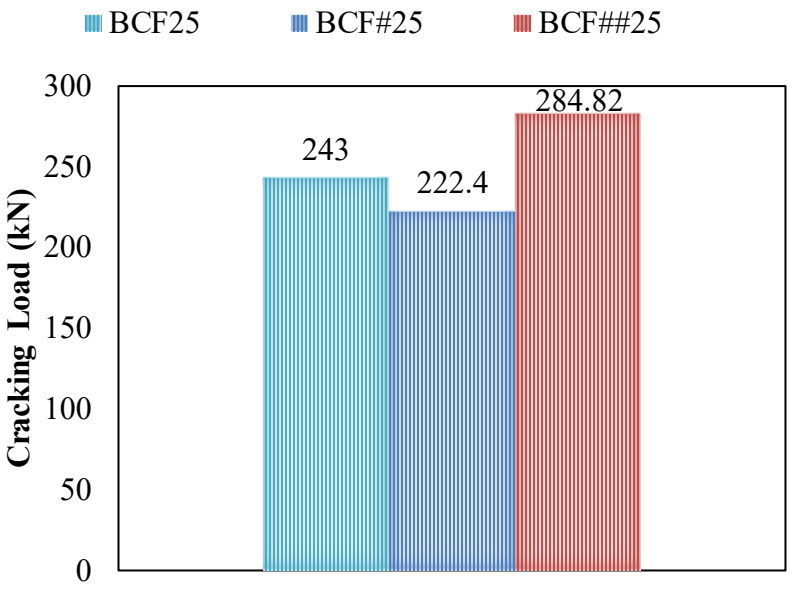

(b)

Figure 4.11: Cracking and ultimate load of curved steel reinforcement beams with different compressive strength

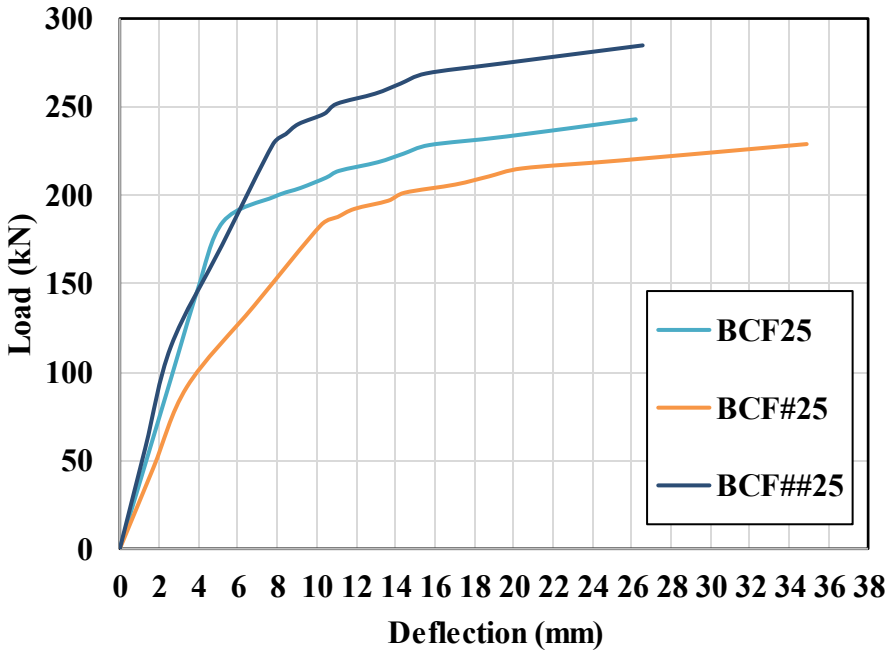

Figure 4.12: Load deflection curve of curved steel reinforcement beams with different compressive strength

4.2.1.2 Flexural Ductility

Figures. 4.14, 4.15 ,4.16 demonstrate the ductility of the RC beam. Concrete ductility index refers to the material's ability to undergo substantial deformation without experiencing sudden failure. Ductile concrete structures can exhibit visible deformations, such as cracking and bending under flexural loads. Among the affected variable on the ductility, the presence of steel fibres, can greatly improve the ductility of concrete, which contributes to control and distribute cracking, providing additional strength and preventing sudden failure. This measurement of ductility is obtained by calculating the ratio of the ultimate deflection (Δu) to the yield deflection (Δy) as shown in figure (4.13) [45].

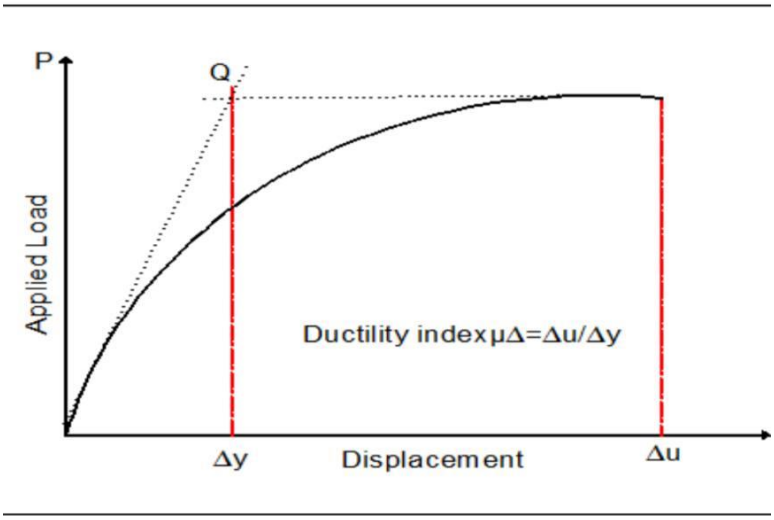

Figure 4.13 : Ductility index calculation

This section presents the results related to the ductility index of reinforced concrete (RC) beams. The control beam, BCFS0, exhibited a ductility index of 3.33. The introduction of curved steel rebars led to notable enhancements in ductility across various models. For Model BCF22, which replaced two straight bars with curved ones, the ductility index increased to 3.51, representing an improvement of 5.4%.This initial enhancement indicates that even a modest change in reinforcement

configuration can positively impact the ductility of the beam. Increasing the number of curved rebars from two to three in Model BCF23 resulted in a more significant improvement in ductility, reaching an index of 3.77, which corresponds to a 12.6% enhancement . This suggests that the additional curved reinforcement further facilitates the beam's ability to deform plastically before failure, enhancing its overall performance. The highest ductility index was observed in Model BCF25, which included five curved rebars. This model achieved a ductility index of 4.07, reflecting a substantial increase of 22.2%. Model BCF1222 achieved a ductility of 4.85, which is a 45.6% increase over the reference model. For the models BCF12, BCF13, and BCF15, which incorporated two, three, and five curved rebars respectively, the enhancements in ductility were 4.8%, 7.8%, and 48.3%. These incremental improvements suggest that while the addition of curved rebars generally contributes to better performance, the benefits may plateau beyond a certain number of curved reinforcements.

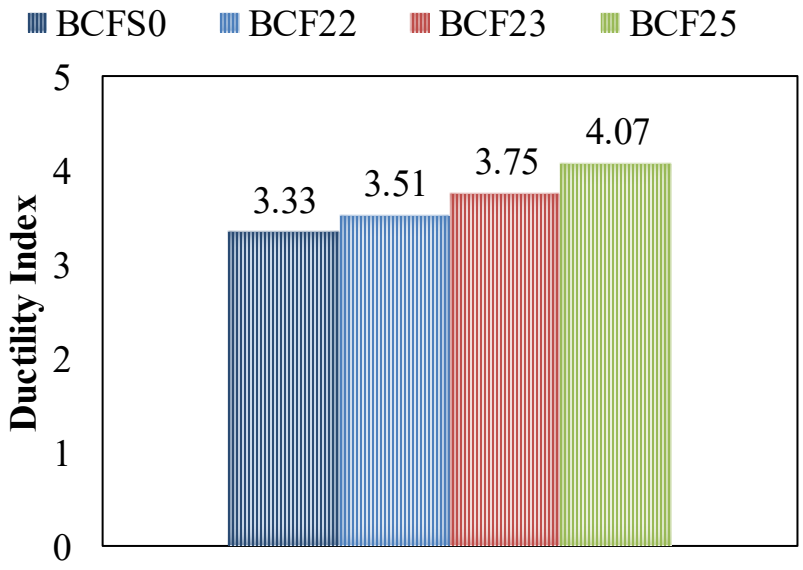

Figure 4.14: Ductility Index of curved steel reinforcement beams

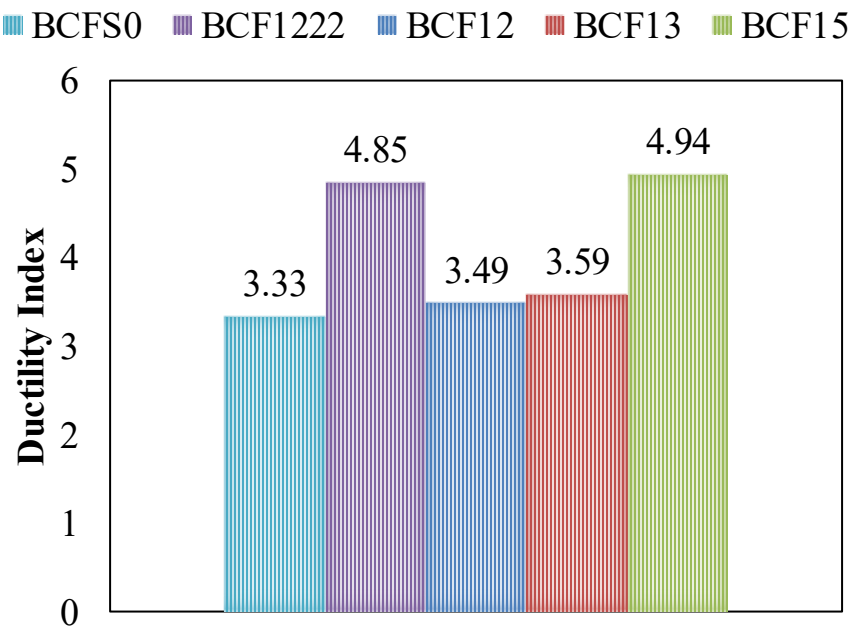

Figure 4.15: Ductility Index of curved steel reinforcement beams with varied number of aligned rebars.

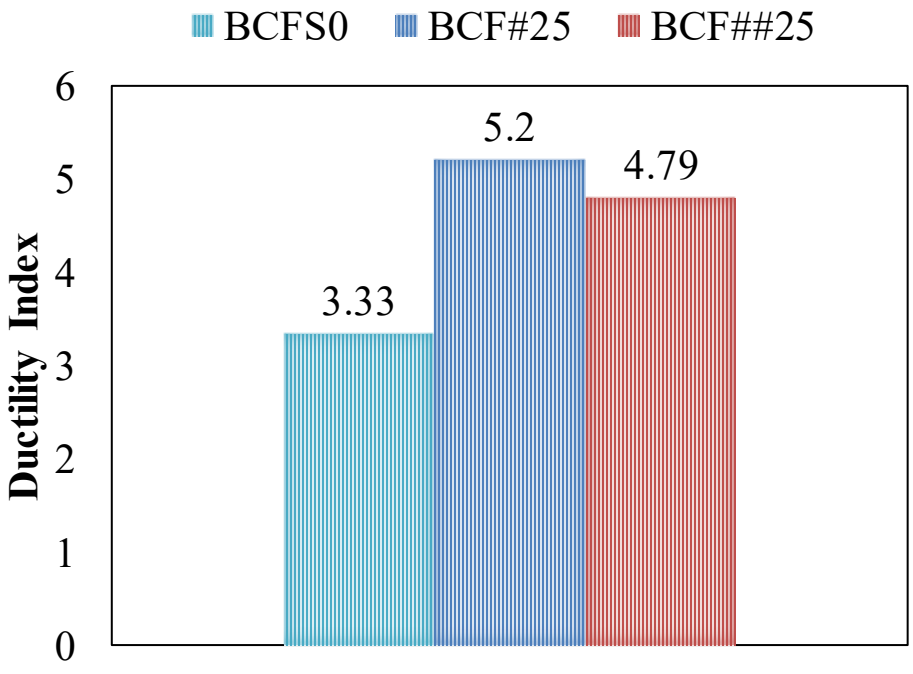

Figure 4.16: Ductility Index of curved steel reinforcement beams with varied compressive strength.

4.2.1.3 Initial Stiffness

Among the various structural properties examined, initial stiffness demonstrated the most notable enhancement due to the inclusion of curved longitudinal steel reinforcement. The curvature of the rebars significantly altered the load-resisting mechanism of the beams, leading to a marked improvement in their initial stiffness. The control beam, BCFS0, which was reinforced with straight longitudinal steel bars, exhibited an initial stiffness of 13.82 kN/mm. This value notably increased to 17.17 kN/mm when two of the straight bars were replaced with curved rebars. The modification represents a substantial improvement and highlights the immediate impact of rebar curvature on the beam's stiffness response. Further increasing the number of curved rebars led to even greater gains. For instance, the specimen BCF23, which incorporated three curved rebars, achieved a 30.7% enhancement in initial stiffness compared to the control beam. Similarly, the BCF-25 specimen, which utilized five curved rebars, exhibited an initial stiffness of 22.8 kN/mm, translating to a 65% increase. These results illustrate a positive correlation between the number of curved rebars and the initial stiffness of the beam, although the rate of improvement may diminish with further additions. Beams reinforced with a rectangular configuration of curved steel bars also showed improvements in initial stiffness, though to a lesser extent. The stiffness values increased to 14.32, 14.97, and 15.08 kN/mm for beams reinforced with two, three, and five bars, respectively, with an average enhancement of approximately 20.3%. While these results are promising, they indicate that the benefits of curvature are more pronounced when applied to longitudinal reinforcements rather than being limited to the overall reinforcement shape. Specimens BCF-12, BCF-13, and BCF-15, incorporating two, three, and five curved rebars respectively, exhibited ductility indices of 16.99, 17.54, and 17.37, corresponding to an average improvement of 25.2%. However, these

results also suggest that the improvement in performance tends to plateau as the number of curved rebars increases beyond a certain point.

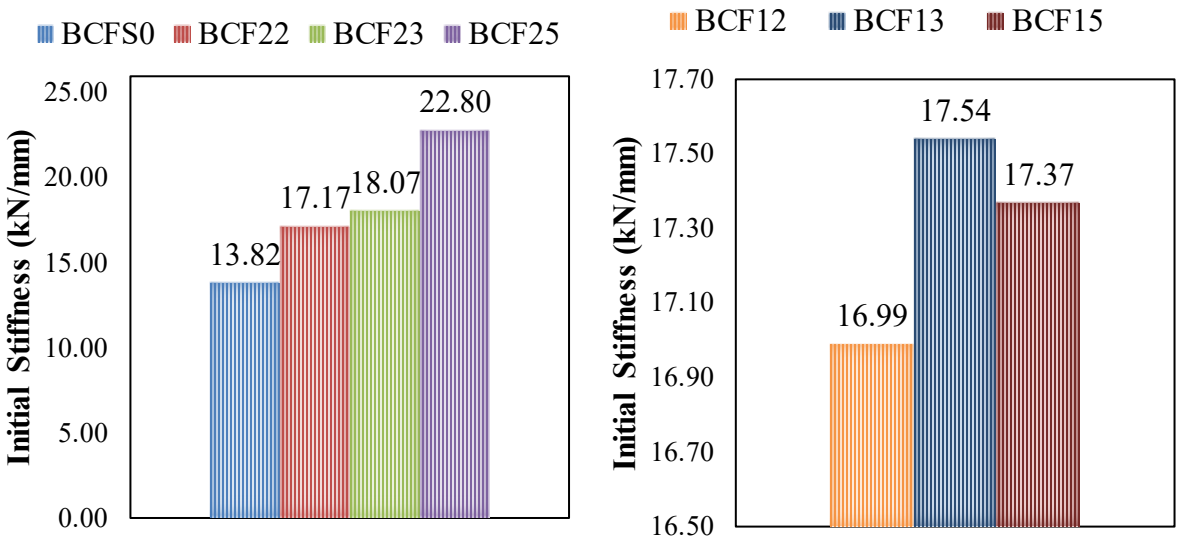

Figure 4.17: Initial Stiffness Results

4.2.1.4 Plastic Rotation Capacity

The ability of a structural member to rotate at a plastic hinge is primarily influenced by three factors: the maximum compressive strain that concrete can withstand, the length over which plastic deformation occurs (commonly taken as equal to the member's effective depth, L_p = d), and the depth of the compression zone, C.

For a plastic hinge forming in the tension zone, the rotational angle, θ, can be approximated using the following relationship:

$$\theta = \frac{\varepsilon_p L_p}{c} \quad \text{.....(3)}$$

Where ε_p represents the additional strain in the concrete that occurs after the steel reinforcement in the section begins to yield [42].

$$\varepsilon_p = \varepsilon_{cu} - \varepsilon_e \quad \text{.....(4)}$$

So that the value of ε_e can be found using the following equation :

$$\varepsilon e = \frac{\sigma}{Ec}$$

where : $E_c = 4700 \sqrt{fc}$, ($f_c = 0.85 \times 30 = 25.5$, $f_c = 0.85 \times 45 = 38.25$, $f_c = 0.85 \times 60 = 51$) , $\varepsilon_{cu} = 0.003$

Table 4-2: Plastic rotation capacity / Mode I

I	Beam remark	E_c MPa	Compressive Strength MPa	ε_e $x10^{-4}$ mm/mm	ε_p $x10^{-3}$ mm/mm	L_p mm	Depth of compression zone	θ rad/mm
1	BCFS0	29067.89	45	1.806	2.8194	296.5	76.230	0.01097
2	BCF22	29067.89	45	1.910	2.809	296.5	76.230	0.010925
3	BCF23	29067.89	45	2.010	2.799	296.5	76.230	0.010887
4	BCF25	29067.89	45	1.952	2.8048	296.5	76.230	0.010909
5	BCF1222	29067.89	45	2.681	2.7319	296.5	76.230	0.010626
6	BCF12	29067.89	45	1.890	2.811	296.5	76.230	0.010934
7	BCF13	29067.89	45	1.951	2.8049	296.5	76.230	0.01091
8	BCF15	29067.89	45	1.932	2.8068	296.5	76.230	0.01092
9	BCF#25	23733.83	30	1.839	2.816	296.5	76.06	0.01098
10	BCF##25	33564.71	60	2.249	2.7751	296.5	76.232	0.010794

4.2.1.5 Energy Absorption

In terms of energy absorption, this property exhibited the most significant enhancement in the structural behaviour of the beams. Which can be represented by the area under force-displacement curve as shown in fig 4.18. The incorporation of curved steel reinforcement led to a notable improvement in energy absorption. The control beam, BCFS0, demonstrated an energy absorption of 1892 kN.mm, which increased to 2505 kN.mm when two straight bars were replaced with curved steel rebar. This represents a commendable enhancement of 32.4%. Further increasing the number of curved rebars from two to three, as seen in specimen BCF23, resulted in an even greater improvement in energy absorption, achieving a remarkable 61% increase. With the highest number of curved rebars in the beam (specimen BCF25), the energy absorption increased to 3492.63 kN.mm, representing an exceptional 84.6% enhancement. Additionally, for beams reinforced with a rectangular configuration of steel bars, energy absorption also improved significantly, with increases of 25.6%, 53.1%, and 71.6% for beams reinforced with two, three, and five curved bars, respectively. This indicates that the curvature of the reinforcement plays a crucial role in enhancing the energy absorption capacity of reinforced concrete beams. Specimen BCF1222 achieved an energy absorption of 3335.8 kN.mm, which is a 76.3% increase over the reference specimen. For the specimens BCF12, BCF13, and BCF15, which incorporated two, three, and five curved rebars respectively, the enhancements in ductility were 4.6%, 33%, and 62.2% respectively in Figure 4.20. These incremental improvements suggest that while the addition of curved rebars generally contributes to better performance, the benefits may plateau beyond a certain number of curved reinforcements. The findings indicate that curving steel reinforcement significantly enhances the energy absorption capacity of RC beams . The initial increase in energy absorption when transitioning from straight to curved

rebars illustrates the effect of reinforcement configuration on the ability of the beam to dissipate energy during loading. The substantial improvements in energy absorption observed with specimens BCF23 and BCF25 highlight the effectiveness of using multiple curved rebars shown in Figure 4.19. The enhanced energy absorption capabilities suggest that the curved configuration allows for better engagement with the surrounding concrete, resulting in improved load transfer and increased resistance to deformation

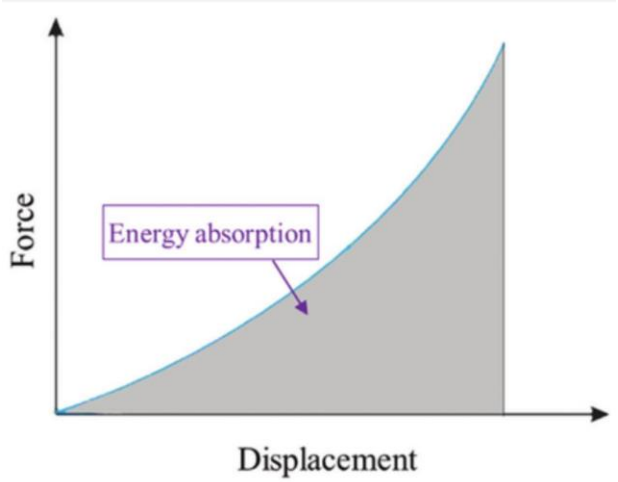

Figure 4.18 : Energy absorption calculation

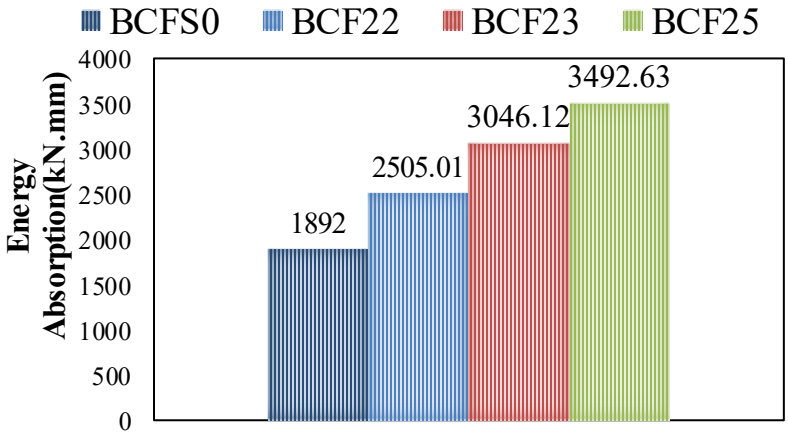

Figure 4.19: Energy absorption of curved steel reinforcement beams.

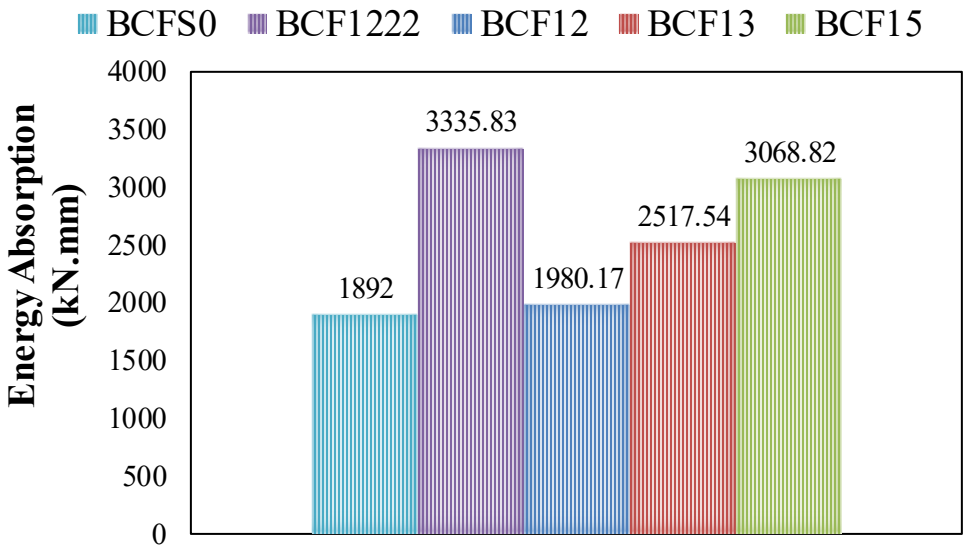

Figure 4.20: Energy absorption of curved steel reinforcement beams with varied number of aligned rebars.

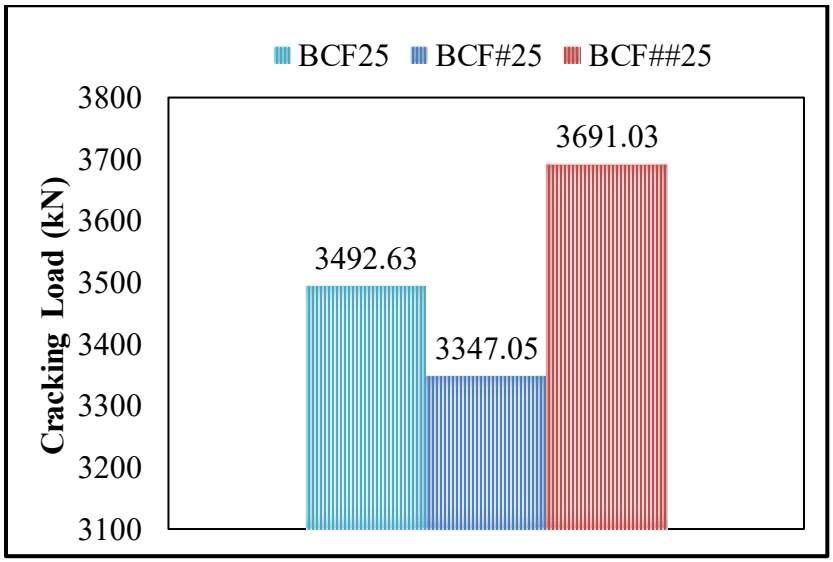

Figure 4.21: Energy absorption of curved steel reinforcement beams with varied compressive strength.

4.2.1.6 Failure Mode

The observations from the crack characteristics and failure mechanisms of the tested beams provide valuable insights into the performance of different

reinforcement types under load. As illustrated in Fig. 4.22 , the behaviour of the beams varied significantly based on the type of reinforcement used, emphasizing the influence of design on structural integrity. The curved steel reinforcement beams (CSRB) demonstrated a unique failure mechanism characterized by the initiation of cracks at the midspan under tension. This behaviour indicates that the curved profile of the steel reinforcement enhances the distribution of tensile stresses, leading to larger and more widely spread cracks compared to conventional reinforced beams. The widening of these cracks under load proposes that the CSRB design allows for greater deformation and energy absorption, which is crucial for preventing sudden failure a desirable trait in seismic applications. Interestingly, the beams with two and three curved steel rebars (BCF22 and BCF23) exhibited a similar cracking pattern, which was notably less severe than that of the control beam (BCSF0). This reduction in crack width indicates that adding curved steel reinforcement can improve the overall ductility and load-bearing capacity of the beams. The most significant findings emerged from beam BCF25, which featured the highest number of curved steel bars. This beam not only experienced larger deformations but also exhibited cracks that extended into the compression region, highlighting a different in failure mode that may enhance the beam's overall structural performance


BCF22


BCF23


BCF25


BCF1222


BCF13

Figure 4.22: Cracks pattern for beams/ Mode I

4.2.2 Rebars aligned Triangularly / Mode II

The study involved testing reinforced concrete beams that utilized triangular reinforcement, with the specimens subjected to failure under static loads. The results from these tests are documented in Table 4-3. The strength values obtained from the tested specimens varied between 185 kN and 231.7 kN, while the displacement values ranged from 23.12 mm to 23.92 mm, as detailed in Table 4-3. The outcomes of these specimens are summarized in relation to all the mechanical properties of reinforced concrete beams that were previously presented and discussed for Mode I. This analysis provides a comprehensive understanding of the performance characteristics associated with the triangular reinforcement configuration.

Table 4-3: Triangular Aligned steel reinforcement RC beams results

II	Beam remark	Cracking Load (kN)	Ultimate load (kN)	Ultimate Deflection (mm)	Ductility index	Energy absorption (kN.mm)	Compressive Strength MPa	Stiffness N/mm
1	BCFS0	55.27	184	20.48	3.33	1892	45	13.82
2	BTF22	52.41	185	23.12	3.56	2376.35	45	14.32
3	BTF23	50.96	192	23.62	3.77	2896.65	45	14.97
4	BTF25	51.36	199	25.64	3.87	3246.67	45	15.08
5	BTF1222	67.21	231.7	23.92	3.97	2732.05	45	19.74

4.2.2.1 Ultimate strength

In this section, the effects of the triangular configuration of steel reinforcement on reinforced concrete (RC) beams are presented. Altering the configuration of the steel rebar to a triangular form impacted the overall behaviour of the RC beams, leading to notable improvements in various performance metrics, including cracking load, ultimate load, deflection, ductility index, and energy absorption. Starting with the control beam, which exhibited a cracking load of 55.27 kN, a significant decrease was observed when straight steel reinforcement was replaced with triangular profile. In Model BTF22, where two steel rebars were substituted with triangular bars, the cracking load decreased by 4.2%. However, the ultimate load remained approximately the same compared to the control beam BCFS0. Increasing the number of triangular rebars from two to three demonstrated further enhancements in

the ultimate load, but also resulted in a decrease in the cracking load when compared to the control beam. The reduction in cracking load was slightly higher at 7.8% in comparison with the model containing two inclined triangular rebars. In terms of ultimate load, there was an enhancement of 4.3%, as shown in Table 4.3. When the number of inclined rebars was increased to five in the second layer of the bottom longitudinal reinforcement, the cracking load further decreased by 7.1%. However, the ultimate strength improved significantly, reaching 199 kN, which is an increase of 8.15%. This represents the highest increase in ultimate strength among variants tested, indicating an improvement in the plastic limit behaviour of the concrete beam while maintaining the same reinforcement ratio. Regarding deflection, the inclination of the steel rebar led to significant increases in deflection. Models with two and three inclined rebars showed enhancements of 12.9% and 15.3%, respectively, as illustrated in Figures 4.23 and 4.24. The highest deflection was recorded for model BCF25, which included the curving of five rebars, depicting an increase of 25.2%, as revealed in Figure 4.25. The results highlight that changing the steel reinforcement configuration to a triangular form can improve the performance of RC beams. The initial decrease in cracking load when transitioning from straight to triangular rebars suggests that the triangular shape may not provide as effective resistance to initial cracking due to potential stress concentrations at the corners of the triangular bars. However, the maintenance of ultimate load capacity in specimen BTF22 indicates that the triangular configuration can effectively distribute loads across the beam, preserving structural integrity despite a reduction in cracking resistance as seen in Fig. 4.24. The highest effect was obtained for specimen BTF1222 was 231.7 by percentage of increase 25.92% in Fig 4.26. The further enhancements in ultimate load with additional triangular rebars suggest that this configuration improves the bond between the concrete and reinforcement, facilitating better load transfer. As the number of triangular rebars increases, the

observed reductions in cracking load alongside improvements in ultimate load capacity indicate a shift in the failure mechanism of the beam. The triangular shape likely allows for better engagement with the surrounding concrete, enhancing the beam's overall performance and ductility. The significant increase in deflection with inclined rebars reflects the inherent flexibility introduced by the triangular configuration. While this flexibility can be advantageous in terms of energy absorption and ductility, it also raises considerations regarding the serviceability of the structure, as excessive deflection can impact usability. In summary, while triangular reinforcement configurations can enhance the mechanical properties of RC beams, it is crucial to carefully balance the number of inclined rebars to optimize performance while managing deflection and cracking behaviour.

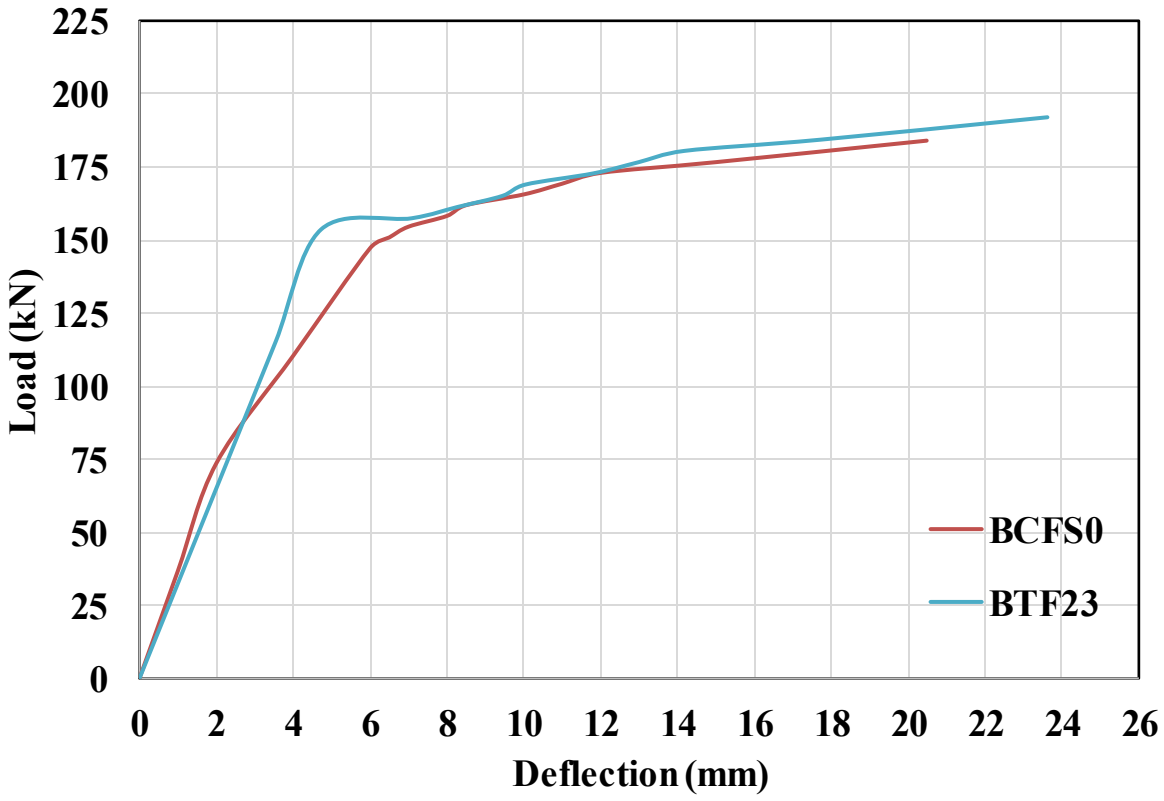

Figure 4.23: Load deflection curve of triangular steel reinforcement beams.

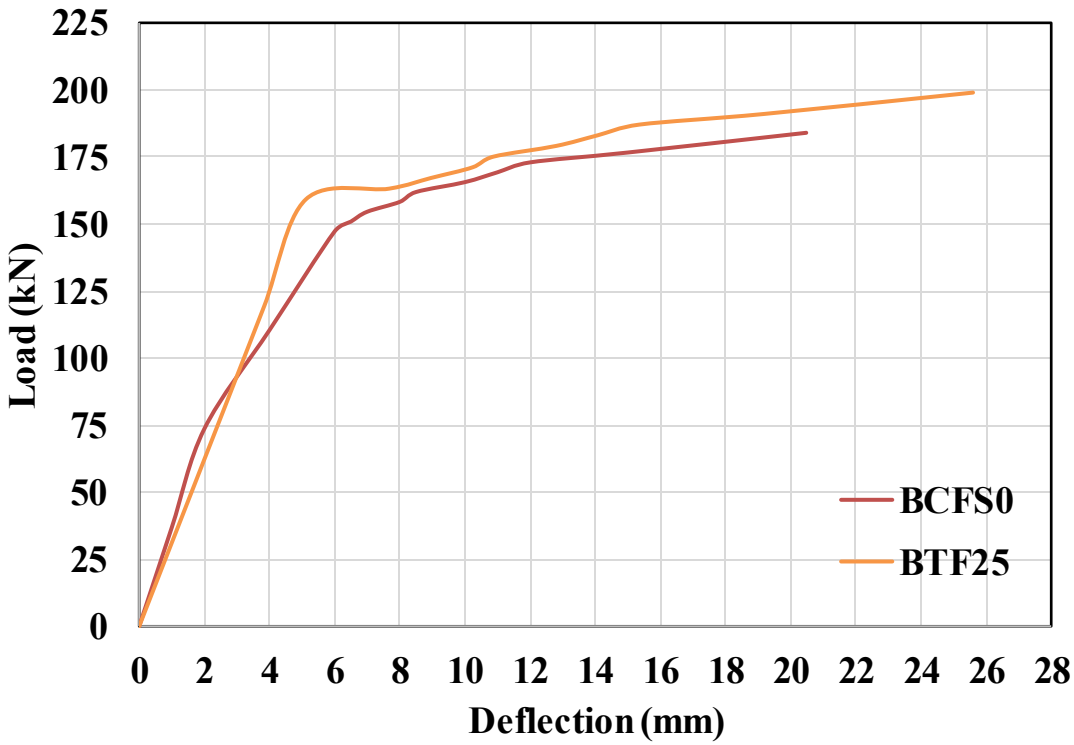

Figure 4.24: Load deflection curve of triangular steel reinforcement beams.

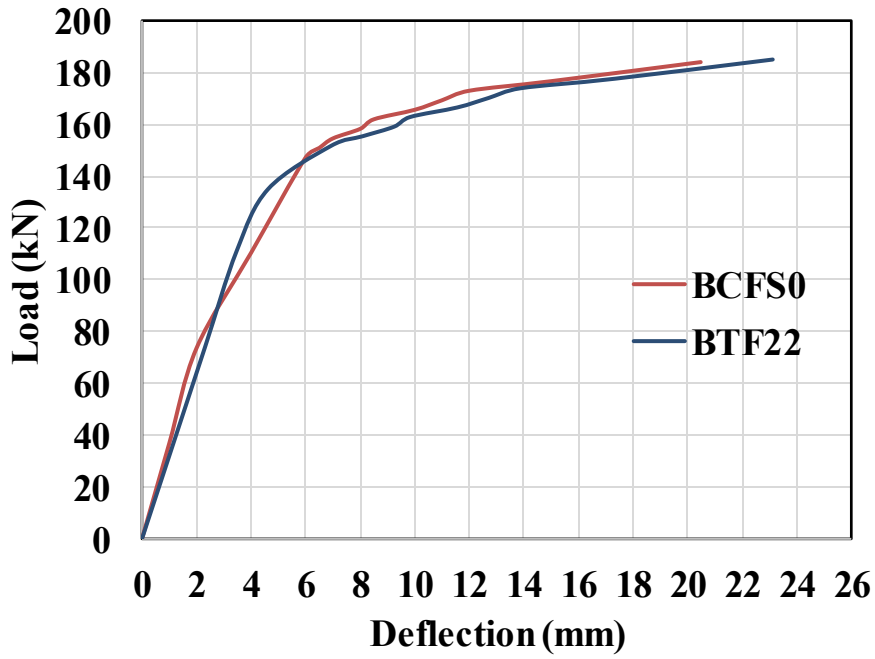

Figure 4.25: Load deflection curve of triangular steel reinforcement beams.

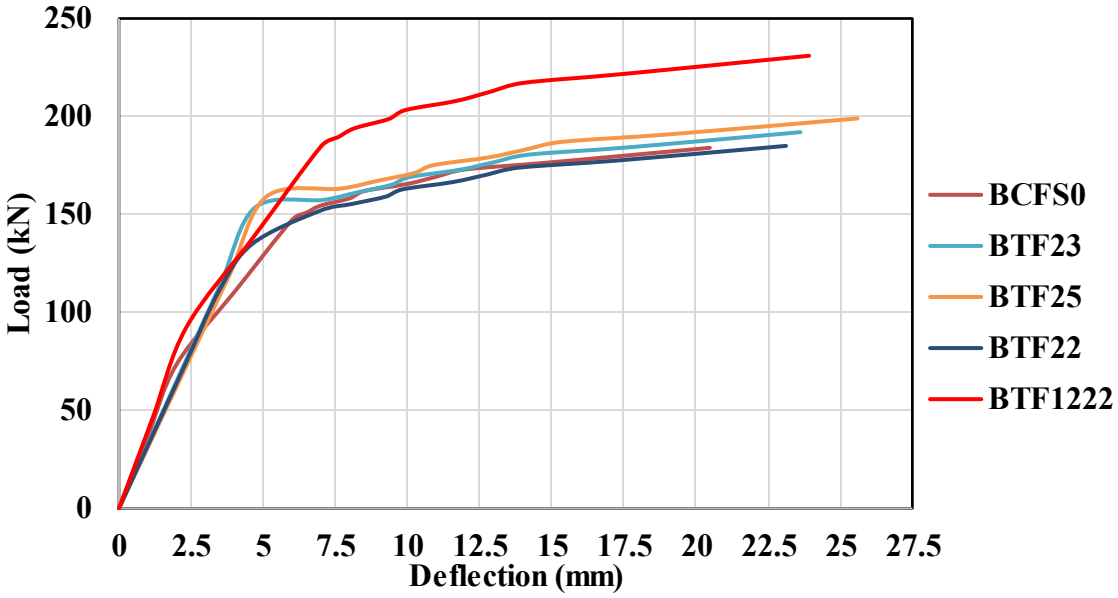

Figure 4.26: Load deflection curve of triangular steel reinforcement beams.

4.2.2.2 Flexural Ductility

Beams reinforced with triangular configuration of steel bars also demonstrated positive enhancements in ductility index. Specifically, beams reinforced with two, three, and five triangular bars exhibited improvements of 6.9%, 13.2%, and 16.2%, respectively. Notably, Specimen BTF1222 achieved a ductility index of 3.97, which represents a significant 19.22% increase compared to the reference sample. These incremental enhancements indicate that while the addition of triangular rebars generally contributes to better performance, the benefits may begin to plateau beyond a certain number of curved reinforcements. In the case of the triangular form of steel reinforcement, Specimens BTF22, BTF23, and BTF25 showcased enhanced ductility with increases of 6.9%, 13.2%, and 16.2%, respectively. These findings emphasize the positive impact of reinforcement configuration on the ductility of reinforced concrete beams, indicating that the design and arrangement of steel reinforcement are crucial factors in determining structural performance.

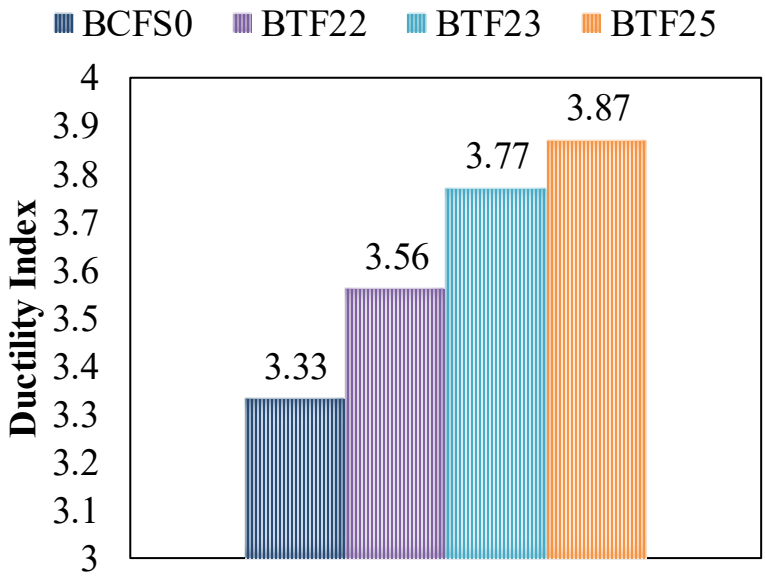

Figure 4.27: Result of ductility index of triangular steel reinforcement beams.

4.2.2.3. Initial Stiffness

Beams reinforced with a triangulare configuration of curved steel bars also showed improvements in initial stiffness, though to a lesser extent. The stiffness values increased to 14.32, 14.97, and 15.08 kN/mm for beams reinforced with two, three, and five bars, respectively, with an average enhancement of approximately 20.3%. While these results are promising, they indicate that the benefits of curvature are more pronounced when applied to longitudinal reinforcements rather than being limited to the overall reinforcement shape. Beams with triangular configurations, specifically specimens BTF22, BTF23, and BTF25, demonstrated even higher enhancements in initial stiffness. This suggests that not only the curvature but also the spatial arrangement of the reinforcement plays a critical role in enhancing structural performance.

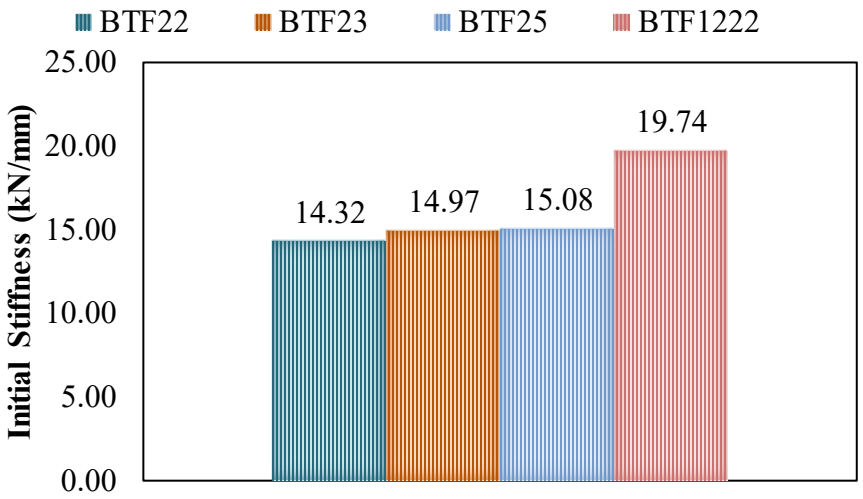

Figure 4.28: Initial Stiffness Results/Mode II

4.2.2.4 Plastic Rotation Capacity

Table 4-4 illustrates the plastic rotation capacities of mode II, which represents triangular reinforcement configuration. The values were calculated using the same method adopted for determining the plastic rotation capacities of the previous models in mode I.

Table 4-4: Plastic rotation capacity / Mode II

I	Beam remark	E_c Mm/mm	Compressive Strength MPa	ε_e $x10^{-4}$ mm/mm	ε_p $x10^{-3}$ mm/mm	L_p mm	Depth of compression zone	θ rad/mm
1	BTF22	29067.89	45	1.712	2.8288	296.5	76.230	0.01100
2	BTF23	29067.89	45	1.656	2.8344	296.5	76.230	0.01102
3	BTF25	29067.89	45	1.678	2.8322	296.5	76.230	0.011015
4	BTF1222	29067.89	45	2.196	2.7804	296.5	76.230	0.01081

4.2.2.5 Energy Absorption

The models featuring triangular steel reinforcement, specifically BTF22, BTF23, and BTF25, demonstrated enhanced energy absorption capabilities, achieving increases of 25.6%, 53.1%, and 71.6%, respectively. These results signify that while both triangular and curved reinforcements contribute positively to energy absorption, the curved reinforcement configuration appears.

To offer more substantial benefits. The increase in energy absorption observed in the models with triangular reinforcement can be attributed to several key factors: The triangular configuration allows for a more effective distribution of tensile stresses across the beam, reducing localized stress concentrations. This leads to a more uniform loading condition, which enhances the energy absorption capacity. he unique geometry of triangular reinforcement contributes to an increase in flexural strength, allowing the beams to undergo larger deformations before failure. This enhancement is crucial for energy absorption, as it enables the structure to dissipate more energy during loading.

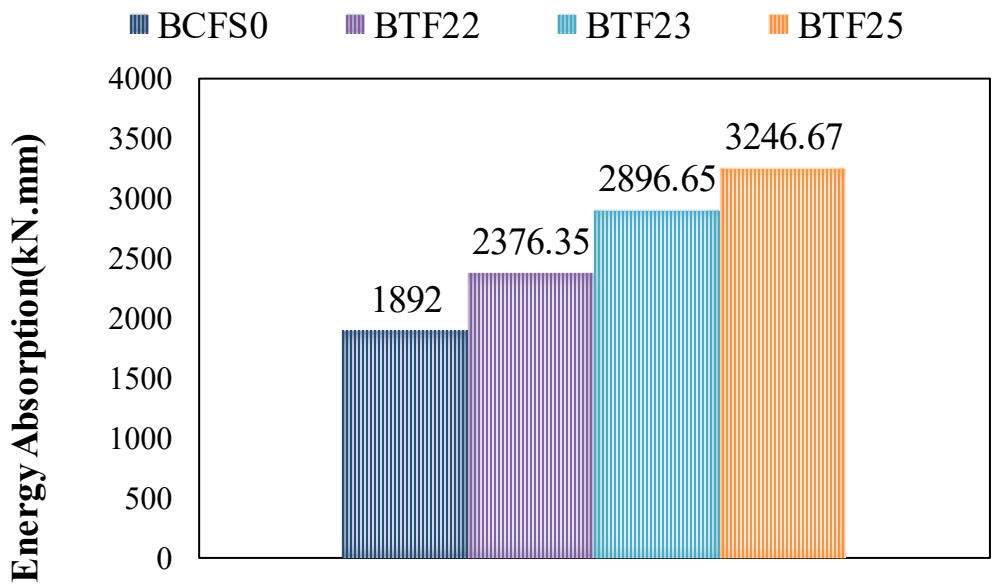

Figure 4.29: Result of Energy absorption of triangular steel reinforcement beams.

4.2.2.6 Failure Mode

The findings regarding the behaviour of triangular steel reinforcement beams under load provide important insights, as illustrated in Figure 4.30. These beams exhibited significant deformation zones, resulting in wider cracks compared to the control beam. However, the severity of these cracks was less than that observed in beams with curved steel reinforcement (CSRB). This suggests that while triangular reinforcement is capable of effectively distributing stresses, it may not be as adept as curved reinforcement in managing crack formation. Additionally, the study highlighted that in specimens with varying compressive strengths, the nature of crack behaviour changed. Specifically, flexural cracks were found to diminish in specimens with higher compressive strength, while the width of the existing cracks increased. This observation indicates that although higher compressive strength can lead to a reduction in the number of cracks, it can also contribute to wider cracks in the areas where they do form. Overall, these findings demonstrate that the triangular rebar configuration has the potential to enhance the overall structural performance of reinforced concrete beams. However, it is noteworthy that the degree of ductility and load-carrying capacity achieved with triangular reinforcement may not reach the same levels as those provided by curved reinforcement.

Figure 4.30: Cracks pattern for beams/ Mode II

CHAPTER FIVE : CONCLUSION AND RECOMMENDATIONS

5.1 General

This conclusion chapter synthesises the findings from the experimental research on the impact of steel reinforcement configurations on the ultimate strength and mechanical properties of reinforced concrete (RC) beams. The study aimed to deepen the understanding of how different reinforcement designs, including curved and triangular configurations, affect the structural behaviour of RC beams under load.

5.2Conclusion

Throughout the research, various parameters such as cracking load, ultimate load capacity, ductility index, and energy absorption were meticulously analysed. The insights gained from this investigation highlight the critical role of reinforcement design in optimising the performance and safety of concrete structures.

[1] The ductility index of RC beams increased with the incorporation of curved rebars, showcasing a direct correlation between reinforcement configuration and ductility. The highest ductility index observed was 4.07 for beams with five curved rebars, reflecting a 22.2% improvement over the control beam. This suggests that curved reinforcement configurations allow for greater deformation capacity before failure, enhancing the overall performance of the concrete structure.

[2] While triangular reinforcement configurations showed improvements in ultimate load capacity and energy absorption Where the results ranged(185 -231.7),(2376.35 – 3246.67) respectively, they were less effective than curved configurations. The transition from straight to triangular rebars resulted in mixed outcomes regarding cracking loads, indicating that triangular shapes may not facilitate optimal stress distribution. Thus, while triangular reinforcement can enhance certain performance metrics, it does not match the benefits provided by curved reinforcement.

[3] The results indicated a positive correlation between compressive strength and the performance of RC beams. Increasing the compressive strength from 30 MPa to 60 MPa led to significant improvements in cracking load from 45.97 to 79.48 and deflection behaviour. The enhanced compressive strength not only improved initial crack resistance but also contributed to reduced deflection under loading conditions, highlighting the importance of material selection in reinforcement design.

[4] The study revealed different failure mechanisms associated with various reinforcement types. Curved steel reinforcement beams exhibited crack initiation at midspan, indicating effective tensile stress distribution. In contrast, triangular reinforcement resulted in wider cracks, suggesting that while they distribute stresses, they do not control crack propagation as effectively as curved reinforcement. Understanding these mechanisms is essential for optimizing beam designs for specific applications.

[5] The findings underscore the importance of thoughtful reinforcement design in ensuring the structural integrity of concrete beams. The ability

of curved and triangular reinforcements to enhance cracking resistance, ductility, and energy absorption indicates that engineers should prioritize these configurations when designing RC structures. This consideration is vital for improving safety and performance in various construction applications.

5.3 Future Research Directions

The study highlights the need for further research on the long-term effects and performance of various reinforcement configurations in different environmental conditions. Future studies could explore the impact of additional variables, such as temperature changes and different loading scenarios, to develop a more comprehensive understanding of how reinforcement design influences the durability and safety of RC structures.

REFERENCES

[1] Christou G, Hegger J, Classen M. Multi-span composite girders with composite dowels–Experimental investigations and design approach to account for the beneficial effect of shear force redistribution along the composite interface. Engineering Structures. 2023 Jun 15;285:115944.

[2] Bayrak O, Sheikh SA. Plastic hinge analysis. Journal of structural engineering. 2001 Sep;127(9):1092-100.

[3] Guyon E. Moment-curvature relationships for reinforced concrete beams. Journal of Structural Engineering. 1976;102(7):1381–1395.

[4] Macchi A. Moment-curvature relationships for concrete elements. Engineering Structures. 1980;2(3):175–184.

[5] Sawyer C. Rotational capacity of reinforced concrete beams. Journal of the New Zealand Concrete Society. 1985;2(1):45–50.

[6] Lee H. Behavior of reinforced concrete beams under cyclic loading. Journal of Structural Engineering. 1989;115(12):3066–3082.

[7] Baker ALL. Ultimate load theory for structural analysis. Journal of Structural Engineering. 1991;117(10):3034–3053.

[8] Gartner E. Moment-rotation relationships for reinforced concrete. ACI Structural Journal. 2000;97(5):689–695.

[9] Bracci JM, et al. Plastic rotation capacity of reinforced concrete beams. ACI Structural Journal. 1997;94(2):125–134.

[10] Priestley MJN, et al. The design of reinforced concrete structures for seismic performance. Journal of Structural Engineering.

2007;133(2):286–295.

[11] Paulay T, Priestley MJN. Seismic Design of Reinforced Concrete and Masonry Buildings. Wiley; 1992.

[12] Park R, Paulay T. Reinforced Concrete Structures. Wiley; 1975.

[13] CEB-FIP. Design of Concrete Structures. Comité Euro-International du Béton; 1990.

[14] CEB-FIP. Model Code 2010. International Federation for Structural Concrete; 2013.

[15] Mendis P. Plastic hinge lengths of standard and high-strength concrete under flexure. Journal of Structural Engineering. 2001;127(2):155-162.

[16] ACI Committee 428. Plastic hinge lengths for reinforced concrete flexural members. ACI Materials Journal. 2000;97(6):714-721.

[17] Mendis P. Effects of softening on hinge length. Journal of Structural Engineering. 1986;112(5):1013-1021.

[18] Mendis P. Softening behavior of standard strength and high-strength concrete structures. Journal of Concrete Research. 2000;52(8):1035-1045.

[19] Rajesh R, et al. Flexural, axial load, and elongation response of plastic hinges in reinforced concrete members. Journal of Reinforced Plastics and Composites. 2007;26(15):1537-1551.

[20] Zhao J, et al. Length of the plastic hinge in reinforced concrete flexural members. Engineering Structures. 2011;33(9):2504-2513.

[21] Hillerborgi, A"Fracture mechanics concepts applied to moment capacity and rotational capacity of reinforced concrete beams," Engineering Fracture Mechanics, vol. 35, pp. 233-240, 1990.

[22] Palanivel K, Sekar A. Flexural and plastic hinge behavior of GFRP

confined composite beams. Materials and Structures. 2013;46(12):1971-1986.

[23] Oudah A, El-Hacha R. Slotted-beam specifications to reposition the center of rotation at beam-column joints. Journal of Structural Engineering. 2014;140(5):04014008.

[24] Ou Y, Nguyen T. Length of plastic hinges of deteriorated reinforced concrete beams. Journal of Structural Engineering. 2014;140(9):04014064.

[25] Pham H, Hao H. Impact behavior of reinforced concrete beams under slow impact velocity. Engineering Structures. 2017;132:360-369.

[26] Oudah A, El-Hacha R. Relocation of plastic hinges in concrete structures using the double-slotted-beam method. Journal of Structural Engineering. 2017;143(2):04016231.

[27] Pokhrel K, Bandelt J. Plastic hinge behavior and rotation capacity in reinforced ductile concrete flexural elements. Journal of Structural Engineering. 2019;145(4):04019014.

[28] Kwan, A. K. H., Ho, J. C. M. and Pam, H. J., "Effects of concrete grade and steel yield strength on flexural ductility of reinforced concrete beams," Australian Journal of Structural Engineering, vol. 5, pp. 1-20, 2004.

[29] Farouk M, Khalil A. Analytical investigation of plastic hinge rotation in flexural members. Engineering Structures. 2019;199:109582.

[30] Somer M. Static load failure patterns of RC beams with varying plastic hinge lengths. Journal of Structural Engineering. 2019;145(8):04019067.

[31] Sayed M, et al. Investigation of different Lp equations on nonlinear structural response of RC frames. Journal of Structural Engineering.

2023;149(4):04023018.

[32] Jassim Kadhim. Structural behavior of simply supported reinforced concrete beams with non-prismatic flanges ;2019

[33] Iraqi Standard 5/1984. Portland Cement Specification.

[34] ASTM C191. Standard Test Methods for Time of Setting of Hydraulic Cement by Vicat Needle.

[35] ASTM C136. Standard Test Method for Sieve Analysis of Fine and Coarse Aggregates.

[36] ASTM C494-99. Standard Specification for Chemical Admixtures for Concrete.

[37] ASTM A615. Standard Specification for Deformed and Plain Billet-Steel Bars for Concrete Reinforcement.

[38] ASTM C143. Standard Test Method for Slump of Hydraulic-Cement Concrete.

[39] ASTM C496. Standard Test Method for Splitting Tensile Strength of Cylindrical Concrete Specimens.

[40] ASTM C78-02. Standard Test Method for Flexural Strength of Concrete (Using Simple Beam with Third-Point Loading).

[41] BS 1881, P. 116. (1989). Method for determination of compressive strength of concrete cubes. In British Standards Institution (p. 3),

[42] Hassoun, M. N., & Al-Manaseer, A. (2020). Structural concrete: theory and design. John wiley & sons.

Appendix

For two layer d = 350 - 25 - 8 - 8 - 12.5 = 296.5

$f_c = 0.85\ f_{cu}$

$\beta_1 = 0.85$ for $f_c < 28$ Mpa $\beta_1 = 0.85 - 0.05\left(\frac{f'c-28}{7}\right)$ $f_c > 28$ Mpa

$\rho_{max} = 0.85 \times \beta_1 \times \frac{fc}{fy}\left(\frac{\varepsilon u}{\varepsilon u + 0.004}\right)$

let $\rho = 0.6\ \rho_{max}$

$\rho_{min} = \frac{1.4}{fy} = \frac{1.4}{400} = 3.5 \times 10^{-3}$

$\rho_{max} > \rho > \rho_{min}$ ..... OK

$As = \rho\ b\ d$

$A_{bar} = \frac{\pi}{4} \times (8\text{ mm})^2 = 50.24\text{ mm}^2$

No. of bars $= \frac{As}{A_{bar}}$

	f_c	β_1	ρ_{max}	ρ
C 30	25.5	0.85	19.7×10^{-3}	11.82×10^{-3}
C 45	38.25	0.78	27.17×10^{-3}	16.302×10^{-3}
C60	51	0.69	32.04×10^{-3}	19.224×10^{-3}

use 10 Φ 8 at two layers

الخلاصة

تناولت هذه الدراسة التحقيق في تأثير شكل حديد التسليح على الخصائص الميكانيكية والقوة القصوى للعتبات الخرسانية المسلحة، مع تركيز خاص على تعزيز المتانة وقدرة امتصاص الطاقة. نظرًا للهشاشة المتأصلة في الخرسانة، هدفت هذه الدراسة إلى استكشاف كيف يمكن للأنماط الهندسية المختلفة للتسليح أن تحسن بشكل كبير الأداء الإنشائي تحت الأحمال. تم إجراء سلسلة من الاختبارات التجريبية على أربع عشرة كمرة خرسانية مسلحة بسيطة التثبيت، خضعت لحملين مركزيين نقطيين. صممت الكمرات بكميات وتكوينات مختلفة من التسليح الطولي، بما في ذلك الأشكال المستقيمة والمنحنية والمثلثة. أظهرت النتائج مدى واسعًا في قدرات الحمل القصوى، تتراوح بين 184 كيلو نيوتن و284.82 كيلو نيوتن، مع هطول بين 20.48 ملم و34.88 ملم. كان تأثير التسليح الفولاذي المنحني ملحوظًا بشكل خاص، حيث أدى إلى تحسن واضح في الحمل الأقصى ومؤشر المطيلية. أظهرت العتبة المسلحة بخمسة قضبان منحنية زيادة بنسبة 32% في قدرة الحمل القصوى ومؤشر مطيلية بلغ 4.07، مما يعكس تحسنًا بنسبة 22.2% مقارنة بالعتبة المرجعية. يكشف التحليل كذلك أن تكوين التسليح يلعب دورًا محوريًا في أداء العتبات الخرسانية المسلحة. وجد أن شكل التسليح المنحني يحسن بشكل كبير كلًا من أحمال التشقق والأحمال القصوى، مما يشير إلى أن هذه الهندسة تعزز التماسك بين الخرسانة والفولاذ، مما يسهل توزيع حمل أفضل ومقاومة أعلى للتشقق الأولي. في المقابل، أسفرت اشكال التسليح المثلثة عن مقاييس أداء إجمالية أقل، على الرغم من أنها ما زالت توفر بعض الفوائد من حيث السلامة الإنشائية. كما تحسنت قدرة امتصاص الطاقة، وهو عامل حاسم في تقييم مرونة المنشآت، بشكل ملحوظ باستخدام القضبان المنحنية. بلغت أقصى قدرة ملحوظة لامتصاص الطاقة 3492.63 كيلو نيوتن.ملم في العتبة المسلحة بخمسة قضبان منحنية، مما يشير إلى زيادة بنسبة 84.6% عن العتبة المرجعية. تسلط هذه الدراسة الضوء على فعالية التسليح المنحني في تبديد الطاقة أثناء التحميل، مما يحسن بالتالي مرونة المنشأ ضد القوى الديناميكية. بالإضافة إلى ذلك، تم استكشاف العلاقة بين مقاومة الضغط والأداء الميكانيكي. أظهرت المواد ذات مقاومة الضغط الأعلى تحسنًا في كل من حمل التشقق وقدرة الحمل القصوى، مما يؤكد أهمية قوة المواد في تحديد الفعالية الإجمالية للهياكل الخرسانية المسلحة. تشير النتائج إلى وجود تأثير تآزري بين انحناء التسليح ومقاومة ضغط الخرسانة، يعززان معًا السلامة الإنشائية والقدرة على تحمل الأحمال للعتبات. كما تناولت الدراسة أنماط الانهيار المرتبطة باشكال التسليح المختلفة. أظهرت العتبات ذات التسليح المنحني انتشارًا أكبر للشقوق ومرونة أعلى، مما يشير إلى تحول في آليات الانهيار يساهم في تحسين الأداء الإنشائي. على العكس من ذلك، أدى التسليح المثلث إلى شقوق أوسع، مما يظهر فعالية أقل في التحكم في انتشار الشقوق مقارنة بالاشكال المنحنية.

في الختام، قدمت هذه الأطروحة رؤى حول التأثيرات الكبيرة لشكل التسليح على الخصائص الميكانيكية للكمرات الخرسانية المسلحة. قد تساهم النتائج في إثراء المعرفة في مجال الهندسة الإنشائية، خاصة في تعزيز متانة وقدرة امتصاص الطاقة للهياكل الخرسانية.

جمهورية العراق
وزارة التعليم العالي والبحث العلمي
كلية الهندسة/ جامعة ميسان
قسم الهندسة المدنية

تعزيز أداء الأنحناء للعتبات الخرسانية المسلحة بأشكال مختلفة لحديد التسليح

رسالة
مقدمة الى كلية الهندسة في جامعة ميسان
كجزء من متطلبات الحصول على درجة الماجستير في علوم الهندسة المدنية / الانشاءات

اعداد الطالب

فاطمة عبود كريم

بكالوريوس هندسة مدني 2020

بأشراف

الاستاذ الدكتور: سعد فهد رسن

حزيران 2025 **ذو الحجة 1446**